BSGF - Earth Sciences Bulletin 2021, 192, 30

https://doi.org/10.1051/bsgf/2021020

BSGF Earth Sciences Bulletin

***Special Issue Orogen lifecycle: learnings and perspectives from Pyrenees, Western Mediterranean and analogues ed. O. Lacombe, S. Tavani, A. Teixell, D. Pedreira and S. Calassou (Guest editors)***

Available online at: www.bsgf.fr

OPEN ACCESS

# Late Pliocene-Pleistocene incision in the Ebro Basin (North Spain)

Vincent Regard[1,*], Arnaud Vacherat[1], Stéphane Bonnet[1], Frédéric Mouthereau[1], Jesper Nørgaard[2] and Mads F. Knudsen[2]

[1] GET, University of Toulouse, UPS (OMP), CNRS, IRD, CNES, 14 avenue Edouard Belin, 31400 Toulouse, France
[2] Department of Geoscience, Aarhus University, Aarhus, Denmark

Received: 3 December 2020 / Accepted: 12 May 2021 / Publishing online: 7 June 2021

**Abstract –** The Ebro Basin constitutes the central part of the southern foreland of the Pyrenees. It was endorheic during the Cenozoic and accumulated sediments. By the end of the Miocene, erosion and river incision reconnected the basin to the Mediterranean Sea, establishing a post-opening drainage network. Those rivers left terraces that we study in this work. We first synthesize previous works on river terraces that are widely dispersed in the basin. We provide new age constraints, up to 3 Ma, obtained thanks to cosmogenic nuclides using both profile and burial methods. We derive a unified fluvial terrace chronology and a homogenized map of the highest terraces over the entire Ebro Basin. The dated terraces labeled A, B, C, D, and E are dated to 2.8 ± 0.7 Ma, 1.15 ± 0.15 Ma, 850 ± 70 ka, 650 ± 130 ka, and 400 ± 120 ka, respectively. The chronology proposed here is similar to other sequences of river terraces dated in the Iberian Peninsula, around the Pyrenees, and elsewhere in Europe. The oldest terraces (A, B, C) are extensive, indicating they form a mobile fluvial network while from D to present, the network was stable and entrenched in 100 to 200 m-deep valleys. The transition from mobile to fixed fluvial network is likely to have occurred during the Middle Pleistocene Transition (MPT, between 0.7 and 1.3 Ma), when long-period/high-intensity climate fluctuations were established in Europe. We estimate that between 2.8–1.15 Ma and present, the incision rates have tripled.

**Keywords:** Ebro Basin / Middle Pleistocene transition / Neogene / fluvial terraces / Pyrenees / cosmogenic nuclides

**Résumé – Incision dans le Bassin de l'Ebre (nord de l'Espagne) entre la fin du Pliocène et le Pléistocène.** Le bassin de l'Ebre constitue le centre du piémont sud-pyrénéen. Il a été endorhéique et a accumulé une épaisseur importante de sédiments au cours du Cénozoique. Vers la fin du Miocène, l'érosion et l'incision fluviale ont reconnecté le bassin à la mer Méditerranée, en établissant un nouveau réseau de drainage. Les rivières constituant ce réseau ont laissé des terrasses que nous étudions dans le cadre de ce travail. Nous faisons d'abord une synthèse des travaux antérieurs sur les terrasses fluviales, qui sont largement dispersées dans le bassin. Ensuite, nous fournissons de nouvelles contraintes d'âge, jusqu'à 3 Ma, obtenues grâce aux nucléides cosmogéniques utilisant à la fois des méthodes de profil d'exposition et d'enfouissement. Enfin, nous en déduisons une chronologie unifiée des terrasses fluviales et une carte homogénéisée des terrasses les plus hautes sur l'ensemble du bassin de l'Ebre. Les terrasses, que nous notons A, B, C, D et E, sont datées respectivement de 2,8 ± 0,7 Ma, 1,15 ± 0,15 Ma, 850 ± 70 ka, 650 ± 130 ka et 400 ± 120 ka. La chronologie proposée ici est similaire à d'autres séquences de terrasses fluviales datées dans la péninsule ibérique, autour des Pyrénées, et ailleurs en Europe. Les terrasses les plus anciennes (A, B, C) sont étendues, ce qui témoignent d'un réseau fluvial mobile alors que depuis la formation des terrasses D jusqu'à aujourd'hui, le réseau était stable et canalisé le long de vallées de 100 à 200 m de profondeur. Le passage d'un réseau fluvial mobile à un réseau fluvial fixe s'est probablement produit pendant la transition du Pléistocène moyen (entre 0,7 et 1,3 Ma), lorsque des fluctuations climatiques de longue période et de forte intensité ont été établies pour les rivières européennes. Nous estimons qu'entre 2,8 et 1,15 Ma et la période actuelle, les taux d'incision ont triplé.

**Mots clés :** Bassin de l'Ebre / transition du Pléistocène Moyen / Néogène / terrasses fluviales / Pyrénées / nucléides cosmogeniques

*Corresponding author: Vincent.regard@get.omp.eu

## 1 Introduction

Intracontinental endorheic basins (or closed basins) occupy ~20% of the Earth's land surface. They develop mostly in response to the tectonic uplift of surrounding ranges, generally under arid climatic conditions (*e.g.* Sobel *et al.*, 2003; García-Castellanos *et al.*, 2003) and are infilled by low-erodible sedimentary rocks. They represent key elements of source-to-sink systems as they preserve eroded products from surrounding catchments and large areas, as for the Tibetan Plateau and Tarim basin (Sobel *et al.*, 2003; Han *et al.*, 2019) or the Altiplano (Fornari *et al.*, 2001; Sobel *et al.*, 2003). Characterized by internally-drained depressions they often record the development of a long-lived lake (Altiplano, Titicaca Lake). The opening of an endorheic basin by the capture of internally-drained rivers and lakes has strong implications on the sediment routing and the evolution of the river landscape (Craddock *et al.*, 2010). Despite the development of analogical and numerical modelling tools, processes by which the river network grows and propagates into a captured endorheic basin remain unclear.

The triangular-shaped Ebro sedimentary Basin in the north-eastern Iberian Peninsula is delimited by the South Pyrenean thrust belt to the north, by the Catalan Coastal Range to the south-east, and by the Iberian Range to the south-west (Fig. 1). The basin recorded a long endorheic stage during Oligocene and Miocene times (Puigdefàbregas *et al.*, 1992; Costa *et al.*, 2010). The re-opening of the Ebro Basin toward the Mediterranean Sea led to an incision wave that propagated within the former endorheic basin and the Catalan Coastal Range (*e.g.* García-Castellanos *et al.*, 2003). The drainage divide delimiting the current Ebro catchment shows numerous evidence of geomorphic disequilibrium suggesting that it is still currently enlarging through drainage network growth, captures, and divide migration (Vacherat *et al.*, 2018; Struth *et al.*, 2019).

In this study, we aim to provide a better resolution of the timing of incision in the Ebro catchment and improving our understanding of the relationships between the morphologic evolution of the Ebro drainage network and the longer-term post-orogenic evolution of the Ebro sedimentary Basin. We first review constraints on Ebro river terrace identifications and ages to propose a consistent terrace chronology scheme throughout the basin. Then, we present new dates for the topmost terraces using *in-situ* produced cosmogenic nuclides ($^{10}$Be and $^{26}$Al), hence providing constraints on the most older, *i.e.* initial, recorded stages of landscape development of the Ebro river network. These new data allow us to track the evolution of the Ebro river network back to the Pliocene.

## 2 Geological setting

### 2.1 Tectonic setting

The Pyrenean orogen resulted from the collision between the Iberian and European continental margins that occurred from the Late Cretaceous to the early Miocene (Choukroune, 1989; Roure *et al.*, 1989; Teixell, 1990, 1996, 1998; Muñoz, 1992; Beaumont *et al.*, 2000; Vergés *et al.*, 2002; Mouthereau *et al.*, 2014). The main period of orogenic growth and exhumation is dated to Eocene-Oligocene (45–30 Ma) (see Yelland, 1990; Morris *et al.*, 1998; Sinclair *et al.*, 2005; Gibson *et al.*, 2007; Jolivet *et al.*, 2007; Rushlow *et al.*, 2013; Labaume *et al.*, 2016). The South Pyrenees thrust sequence shows that deformation propagated from east to west and from north to south since the Late Cretaceous. This orogenic sequence is reflected, north of the Ebro Basin, in the syn-orogenic tectonic-stratigraphic relationships well preserved in the South Pyrenean Zone (SPZ), a classical thin-skin fold and thrust belt made of Mesozoic to Cenozoic sediments detached in the Triassic evaporites (Muñoz, 1992; Vergés *et al.*, 1995, 2002; Mouthereau *et al.*, 2014; Carola *et al.*, 2015; Saura *et al.*, 2016). It was followed by a post-orogenic phase of exhumation reported throughout the Pyrenees at about 10 Ma (Morris *et al.*, 1998; Fitzgerald *et al.*, 1999; Whitchurch *et al.*, 2011; Fillon *et al.*, 2013, 2020; Mouthereau *et al.*, 2014; Bosch *et al.*, 2016; Monod *et al.*, 2016; Huyghe *et al.*, 2020; see also the review by Calvet *et al.*, 2020).

The Iberian chain, south of the Ebro Basin, forms a NW-SE trending doubly vergent intraplate mountain belt. It results from the tectonic inversion of Mesozoic rift basins comprising from east to west the Columbrets, Asturian, Basque-Cantabrian, Maestrat, south Iberian, and Cameros basins (Roca and Guimerà, 1992; Salas and Casas, 1993; Salas *et al.*, 2001; Etheve *et al.*, 2018). Constraints on the recent exhumation pattern of the Iberian chain mainly come from the Cameros basin (Del Rio *et al.*, 2009; Rat *et al.*, 2019). ZFT thermochronological constraints show a minimum age for the inversion initiation of the Cameros basin at ~60 Ma, which is coincident or slightly predates the widespread increase in exhumation rates during the Eocene documented in the Pyrenees. The main exhumation phase is recorded in the Cameros basin at 35–25 Ma coevally with the Pyrenees and the Cantabrian belt (Fitzgerald *et al.*, 1999; Fillon *et al.*, 2016). The increase of exhumation is temporally consistent with the closure of the connection of the Ebro Basin with the Atlantic Ocean by 36 Ma, leading to the deposition of thick alluvial sediments (Costa *et al.*, 2010). As in the Pyrenees, this exhumation was followed by a Miocene period of planation that resulted in the paleosurfaces still visible on top of the Iberian chain (Calvet *et al.*, 2015). The deposition of late Miocene conglomerates, sealing the main Cameros thrust, was followed by erosion after ~9 Ma (Rat *et al.*, 2019). This result is in agreement with the regional drainage reorganization described throughout the Ebro Basin (García-Castellanos *et al.*, 2003; Fillon *et al.*, 2013, 2020).

The Catalan Coastal Ranges (CCR), located between the Ebro Basin and the Valencia Trough, formed by the tectonic inversion of Mesozoic rift basins during the Paleogene, contemporaneously with the Pyrenean orogeny (Salas *et al.*, 2001; Gaspar-Escribano *et al.*, 2004). From Late Oligocene onward, extension in the Valencia Trough associated with opening of the Gulf of Lion led to the development of ENE-WSW to NE-SW-striking horst and graben, triggering uplift (Lewis *et al.*, 2000; García-Castellanos *et al.*, 2003).

During the Late Eocene, uplift in the Western Pyrenees (Muñoz *et al.*, 1986; Puigdefàbregas *et al.*, 1992) closed the Ebro Basin. This resulted in a sudden increase of sedimentation rates and continentalization of the endorheic basin (Costa *et al.*, 2010). The deposition of a large amount of coarse alluvial deposits (Coney *et al.*, 1996; Babault *et al.*, 2005b) from Bartonian to Late Oligocene (Beamud *et al.*, 2003, 2011)

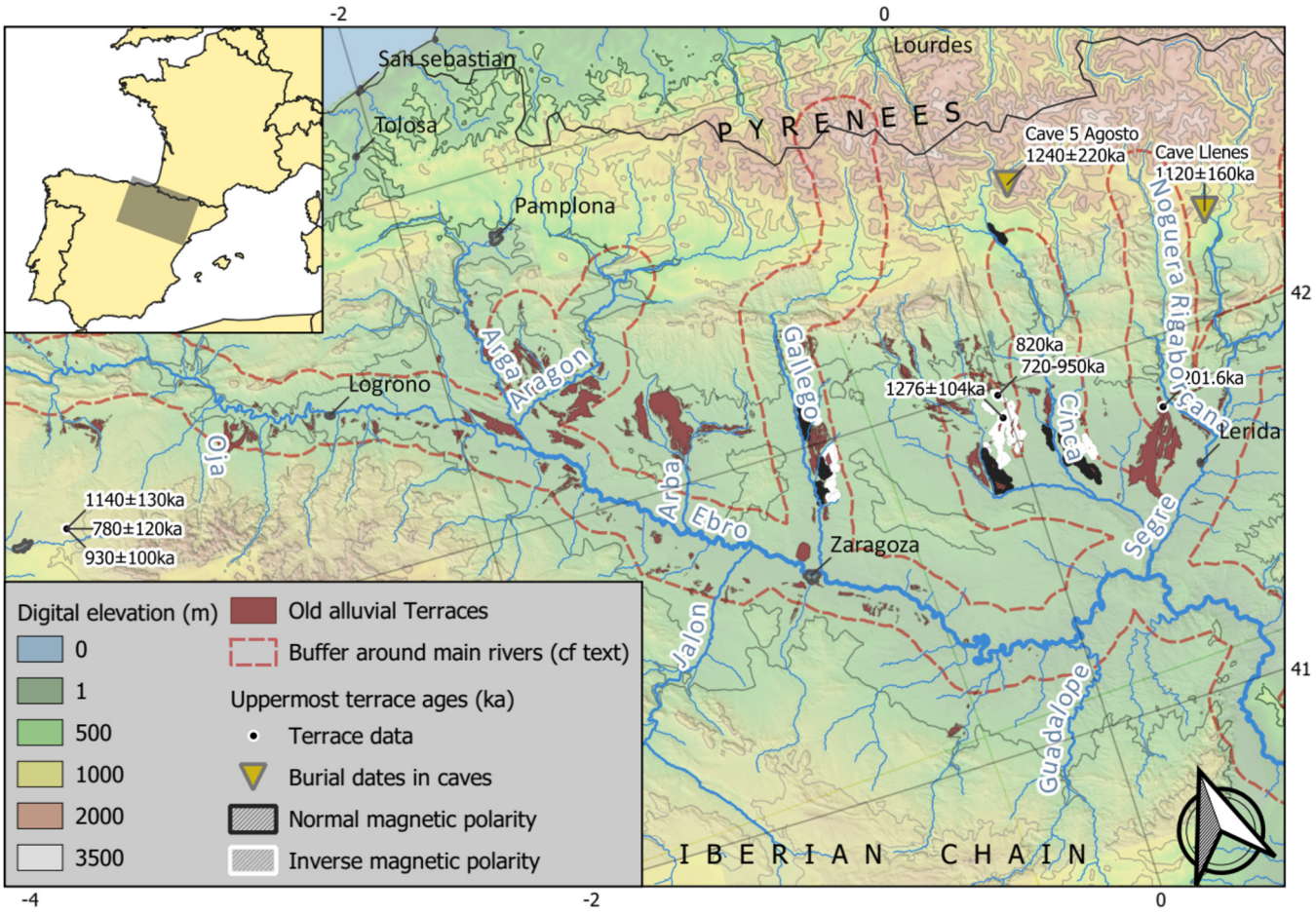


**Fig. 1.** Topographic map of Ebro Basin showing the position of topmost terraces together with their ages and paleomagnetic polarity data (Benito *et al.*, 1998; Moreno *et al.*, 2012; Calle *et al.*, 2013; Stange *et al.*, 2013a; Duval *et al.*, 2015; Lewis *et al.*, 2017). Two burial ages in caves from Genti (2015) which are likely related to these topmost terraces are also indicated. The 10-km wide buffer around the rivers serve for the drawing of Figure 6. An enlarged version of this figure can be found on Zenodo (https//doi.org/10.5281/zenodo.4721256).

filled the paleovalleys that developed at the front of the South-Pyrenees (Vincent, 2001). Such conglomeratic bodies are also observed against the Catalan Coastal Range and the Iberian Range. The center of the Ebro basin became a long-lived lake filled with lacustrine and sandy deposits during the Oligocene and the Miocene (Pérez-Rivarés *et al.*, 2002, 2004; García-Castellanos *et al.*, 2003; García-Castellanos, 2006; Larrasoaña *et al.*, 2006; Vázquez-Urbez *et al.*, 2013).

In the Pyrenees, in addition to the low temperature thermochronology data already mentioned, post-10 Ma uplift is suggested by geological data (Calvet *et al.*, 2020) including recent paleoelevation estimates (*e.g.* Huyghe *et al.*, 2020). This uplift is consistent with the reconstruction of the evolution of river profiles suggesting a post-30 Ma incision of the whole of Iberia (Conway-Jones *et al.*, 2019). In the absence of significant crustal shortening, the drivers of this post-10 Ma uplift are heavily debated. They include changes related to increasing temperature in the asthenospheric mantle, regional scale mantle flow, lithospheric folding, or magmatic addition in the lithospheric mantle (Cloetingh *et al.*, 2002; Boschi *et al.*, 2010; Faccenna *et al.*, 2014; Conway-Jones *et al.*, 2019; Huyghe *et al.*, 2020).

## 2.2 Timing of Ebro Basin opening to the Mediterranean Sea

The timing and factors controlling the opening of the Ebro basin toward the Mediterranean Sea have long been debated, mainly due to the limited chronological constraints. Extension in the Catalan Coastal Range (CCR) triggered rift flank uplift, which, together with dry climatic conditions, favored the endorheic basin stage (García-Castellanos *et al.*, 2003). This extension finally resulted in the Valencia Trough opening during Miocene (Fontboté *et al.*, 1990; Roca *et al.*, 1990, 1999; Sàbat *et al.*, 1995; López-Blanco, 2002). Coney *et al.* (1996) proposed that the Valencia Trough opening was responsible for the capture of the Ebro paleo-lake. Seismic and sedimentary analysis of the Ebro delta in the Valencia Trough have shown that the first record of siliciclastic sediments coming from the Iberian margin is Serravalian-Tortonian in age (Castellon Group, Evans and Arche, 2002). García-Castellanos *et al.* (2003) then proposed that the age and amount of sediments preserved in the Valencia Trough are consistent with an onset of basin opening between 13 and 8.5 Ma, further facilitated by wetter climatic conditions that increased base level in the paleo-lake. The timing

of basin opening has been refined to 12–7.5 Ma by combining the flexural isostatic compensation of the eroded volume with available constraints on sediment age (García-Castellanos and Larrasoaña, 2015). This timing of basin incision is coherent with low-temperature thermochronological studies reporting AHe cooling ages from the SPZ (Fillon *et al.*, 2013) and AHe ages from the western Axial Zone in the Pyrenees (Bosch *et al.*, 2016; Fillon *et al.*, 2020) documenting post-orogenic exhumation between 9 and 11 Ma. In its lower reaches, the Ebro seems to have crossed the CCR before the Messinian Salinity Crisis (MSC), as evidenced by clasts sourced from the Pyrenees (Arasa-Tuliesa and Cabrera, 2018). The MSC did not lead to the entrenchment of the Ebro at the bottom of a deep canyon, unlike what has been observed for the Nile (Chumakov, 1967) and the Rhone (Loget *et al.*, 2005; Mocochain *et al.*, 2009). This issue was resolved by detailed offshore seismic constraints that document canyons buried offshore in the Ebro delta filled by pre-Messinian sediments (Urgeles *et al.*, 2011). Based on the above arguments, we consider the Ebro Basin opening toward the Mediterranean Sea occurred between 7.5 and 13 Ma (see also Calvet *et al.*, 2020 for a synthesis).

Beyond the issues about the age of incision of the Ebro Basin and whether its capture is related to sediment overfilling or headward retreat incision (García-Castellanos *et al.*, 2003), little is known about the evolution of a river network after the onset of the capture of Ebro basin.

### 2.3 Ebro Basin paleoclimates

At the beginning of our study period, during the Miocene, the climate of the Ebro basin was subtropical and dry (López Martínez *et al.*, 1987; Barrón *et al.*, 2010), favoring the development of endorheic lakes (García-Castellanos, 2006). During the Middle-Late Miocene and Early Pliocene, northern Iberia recorded alternations of cold-wet and hot-dry periods (*i.e.*, Bessais and Cravatte, 1988; Barrón *et al.*, 2010). Afterwards, the Panama Isthmus closure at ~ 3 Ma induced the establishment of the present-day oceanic circulation and global climate (*cf.* Maier-Reimer *et al.*, 1990; Haug and Tiedemann, 1998; Molnar, 2008). This led, during the Quaternary, to more humid and colder climate conditions characterized by dry glacial periods and humid interglacials, especially for the Mediterranean area (Suc and Popescu, 2005; Jiménez-Moreno *et al.*, 2013). Finally, during the Lower-Middle Pleistocene Transition (MPT, ~ 1.3–0.7 Ma), the dominant orbital periodicity changed from 41 ka to 100 ka (Tziperman and Gildor, 2003; Lisiecki and Raymo, 2005; Siddall *et al.*, 2010).

### 2.4 Review of Ebro Basin fluvial terraces, with emphasis on the topmost terraces

In the Ebro Basin, the flights of fluvial terraces along the main rivers and tributaries are widespread and can be organized to first-order into two groups (*e.g.* Lucha *et al.*, 2012). The most elevated terrace levels (Fig. 1), at > 100–150 m above the current river level, consist of widespread and high-elevation pediment surfaces covered by up to ~ 20 m of rounded pebbles of varying lithology. These upper levels are often located at the summit of hillcrests and seem locally disconnected from the present drainage network (*e.g.* Bomer, 1979). On the opposite, below ~ 120 m, most of the terrace levels have a limited extent within modern valleys and along river courses. This morphological break highlights a transition between wandering fluvial systems with efficient lateral planation and beveling capabilities (*e.g.* Cook *et al.*, 2014; Bufe *et al.*, 2016, 2017) to entrenched and more stable river courses (*e.g.* Bomer, 1979). The term "mobile" refers to lateral river mobility, enhancing lateral erosion, whose greatest effect is valley widening up to the beveling of large platforms. For example, the Barbastro-Balaguer anticline has been completely flatten during the setup of these high levels (Lucha *et al.*, 2012) before being subsequently entrenched by the Cinca, Noguera-Ribargorzana, and Segre rivers. The contrasting behaviour of the rivers after this transition is well illustrated by the terraces sequences of the Cinca (Lewis *et al.*, 2017) or Alcanadre rivers (Calle *et al.*, 2013). It may correspond to a transition from a depositional stage under sub-arid conditions, toward a more erosive stage characterized by a more focused incision. This could correspond to the climatic change recorded during the Lower-Middle Pleistocene transition (*e.g.* Stange *et al.*, 2016). The formation of terraces younger than the Middle Pleistocene transition appears to be related to global climatic cycles (*e.g.* Macklin *et al.*, 2002; Santisteban and Schulte, 2007; Arboleya *et al.*, 2008), though other parameters such as uplift may be also important in defining the number of terraces and their altitudinal distribution (Santisteban and Schulte, 2007).

Due to the marked interest in the relationship between the incision and glacial cycles, most previous studies in the Ebro and Duero basins have focused on the lowest terrace system, close to the actual course of the rivers (*e.g.* Lewis *et al.*, 2009; Calle *et al.*, 2013; Stange *et al.*, 2013a, 2013b). In addition, the lower terraces are much easier to date with classical methods like OSL, TL, ESR, $^{10}$Be cosmonuclide, and even $^{14}$C, usually much more efficient for ages under 300 ka (*e.g.*, Fuller *et al.*, 1998; Lewis *et al.*, 2009, 2017; Calle *et al.*, 2013; Stange *et al.*, 2013a; Duval *et al.*, 2015, 2017; Sancho *et al.*, 2016, 2018; Delmas *et al.*, 2018; Soria Jáuregui *et al.*, 2019).

The highest preserved terraces levels in the Ebro and Duero basins, supposed to be the oldest evidence of fluvial incision, have often been considered as regionally coeval based on their elevation only (Bomer, 1979; Julián Andrés, 1996; Santisteban and Schulte, 2007; Lucha *et al.*, 2012). This relative approach is important because dates alone sometimes do not allow deciphering the various terraces. Moreover, these dates are difficult to obtain. They are mainly derived from ESR, magnetostratigraphy, and more recently cosmogenic pairs of nuclides (Fig. 1). In the following paragraphs, we review the labels and dates of these highest levels and the chronological transition toward the lower levels, *i.e.* when the river began to entrench. We adopt a roughly East-West progression, first for the Pyrenean (northern) reaches and then for the southern reaches.

Along the Segre river flowing from the Pyrenees, 8 levels of terraces have been documented (Stange *et al.*, 2013b), as well as in its major tributary, the Noguera Ribagorçana. The three top-most terrace levels are covering the interfluve to the west in between the Noguera Ribagorçana and the Cinca Rivers (the "highest" levels described before; Bomer, 1979; Stange *et al.*, 2013a) but have not been documented along the Segre river. These three top-most terraces are characterized by

important cementation (Bomer, 1979; Delmas, 2019). They lie 110–160 m above the present-day Noguera Ribagorçana river course (Bomer, 1979; Lucha *et al.*, 2012; Stange *et al.*, 2013a). The uppermost level has been dated to be ~200 ka BP by inversion of $^{10}$Be depth profiles by Stange *et al.* (2013a) (Fig. 1), but this date is questioned regarding the inversion technique adopted (Delmas, 2019) and the correlation with the Ebro high fluvial terraces (see below, Bomer, 1979; Lucha *et al.*, 2012). In the upper Noguera Pallaresa, a tributary of the Segre, cave deposits were recently dated using the cosmogenic burial method to ~1.1 Ma ($^{26}$Al,$^{10}$Be pair in Llenes cave, ~100 m above the current river course, Fig. 1) (Genti, 2015).

Along the Cinca river, 10–11 terrace levels are documented (Bomer, 1979; Peña-Monné and Sancho, 1988; Santisteban and Schulte, 2007; Lewis *et al.*, 2009, 2017). The two topmost levels are equivalent to the three topmost levels mentioned to the west of the Noguera Ribagorçana valley. They are labelled Qt1 and Qt2 by Santisteban and Schulte (2007) and are ~180 m and ~130 m, respectively, above the present-day river course. The terrace level immediately below (Qt3 in Santisteban and Schulte, 2007), shows a normal magnetic polarity whereas Qt1 and Qt2 polarities are reverse. In addition, based on the degree of soil weathering, Lewis *et al.* (2017) proposed an age of 401 ± 117 ka for Qt3. Qt5 is dated to 178 ± 21 ka (OSL, Lewis *et al.*, 2009) and Lewis *et al.* (2017) estimate likely ages of 999–1070 ka and 780–999 ka for Qt1 and Qt2, respectively, on the basis of paleomagnetic data. ESR analyses were also performed on these terraces, yielding ages of ~1.3 and ~0.8 Ma for Qt1 and Qt2, respectively (Duval *et al.*, 2015; Sancho *et al.*, 2016). Remnants of Qt1 and Qt2 are located on the interfluve between the Cinca and the Alcanadre rivers (Fig. 1).

The Alcanadre river is the next main river to the west and is a tributary of the Cinca river. 9 terrace levels have been mapped along the Alcanadre river. The two topmost levels, Qt1 and Qt2 were presented in the preceding paragraph. They lie at 160–200 m and 100–190 m, respectively, above the present-day Alcanadre river, and are characterized by inverse magnetic polarity (Calle *et al.*, 2013; also dated with ESR as discussed in the following Duval *et al.*, 2017) (Fig. 1).

The next river to the west is the Gállego river. 10 to 12 terraces are described along its course (Benito *et al.*, 2000; Santisteban and Schulte, 2007 and references; Lewis *et al.*, 2009; Benito *et al.*, 2010). The 5–6 uppermost levels are older than the Brunhes-Matuyama transition. The Brunhes-Matuyama transition is at ~150 m above the current Gállego river (Santisteban and Schulte, 2007). To the south of the city of Zaragoza, the Rio Huerva displays a similar, well-developed terrace sequence up to 150 m above the river course, but not dated (Guerrero *et al.*, 2008). The highest terraces described along the Ebro river course are those found close to Zaragoza (Benito *et al.*, 2000) and 30 km downstream (T1 and T2 ~200 m above the current Ebro course, Guerrero *et al.*, 2013) (Fig. 1). Locally, the terrace sequence is disturbed by karstic processes; this is particularly true in the Zaragoza area (Mensua and Ibañez, 1977; Benito *et al.*, 1998, 2000, Guerrero *et al.*, 2008, 2013). These remarks probably explain that the important Gállego set of terraces do not appear in large-scale correlation (*e.g.*, Santisteban and Schulte, 2007).

The last important tributary sourced from the Pyrenees is the Aragón river. It has been mostly studied in its upper reaches in the mountain, for the glacially-derived terraces (García-Ruiz *et al.*, 2013). Along its course within the Ebro Basin, Bomer (1979) indicates 5 fluvial terraces. The topmost one lies 120–140 m above the present-day river and builds a large plateau testifying for a mobile river when it formed. This terrace is likely equivalent to the large set of terraces found at the top of the Ribagorzana and Cinca valleys (Bomer, 1979). In its lower part, it is highly deformed by diapiric movements (Casas *et al.*, 1994). To the north of the Aragón river, along its Cidacos tributary, an extensive terrace sequence is preserved (Fig. 1). The difference in elevation of the Cidacos terraces appears to increase towards the Ebro Basin.

In the upper reaches of the Ebro river, high terrace levels surrounded by glacis are observed (Soria Jáuregui *et al.*, 2019). In the Duero basin, close to the drainage divide with the Ebro Basin (Vacherat *et al.*, 2018), the highest Arlanzon river terraces T3, T4, and T5, were dated, using ESR, between 1.1 Ma, and ~0.6 Ma (Moreno *et al.*, 2012) (Fig. 1).

To the south, numerous rivers with documented terraces are draining toward the Ebro, like the Najerilla river, which has a well-preserved terrace record composed of 10 levels, but with sparse chronological information (Julián Andrés, 1996) (Fig. 1). The only one southern tributary with chronological data is the Guadalope river whose terrace record comprises 13 levels with some IRSL chronological up to 250 ka BP (Fuller *et al.*, 1996, 1998). Along the Guadalope river, the uppermost terraces, lying ~56 and 81 m above the current river stream, could be equivalent to the topmost terraces along the Cinca and Gállego valleys (Santisteban and Schulte, 2007).

## 3 Methods

### 3.1 Towards a unified model of Ebro terrace succession

There has been a little attempt, so far, to provide a unified model of terrace succession over the Ebro drainage basin. Tentative correlations have been proposed however in some parts of the basin, mainly along the Segre and its tributaries: Alcanadre, Cinca, Noguera Rigaborçana (Bomer, 1979; Alberto *et al.*, 1983; Stange *et al.*, 2013b). Rare correlations between terraces along distant valleys were proposed, like the correlation between the Gállego and Alcanadre river terrace sequences (Mensua and Ibañez, 1977; Lewis *et al.*, 2017) or the one between main river terraces on both sides of the Pyrenees (Delmas *et al.*, 2018; improved from Cordier *et al.*, 2017). No attempt was made to correlate with fluvial terraces further west, probably because of the distance and because the area of Zaragoza and the Gállego valley is disturbed by local deformations produced by the mobilization and dissolution of evaporite (Benito *et al.*, 1998, 2000, Guerrero *et al.*, 2008, 2013).

We have correlated and unified the terrace labels over the entire basin at a scale of 1:50 000 (workflow on Fig. 2). We have first considered individual geographical areas (usually a valley) before to evaluate correlations between the successive locations. At the valley scale, we used georeferenced 1:50 000 geomorphological maps (Mapa Geomorfológico de España a escala 1:50 000 published by IGME; UTM 30 or 31 reference system; info.igme.es/cartografiadigital/tematica/Geomorfologico50.aspx?language=es). These maps contain a detailed mapping of the terraces and a nomenclature in alphabetical

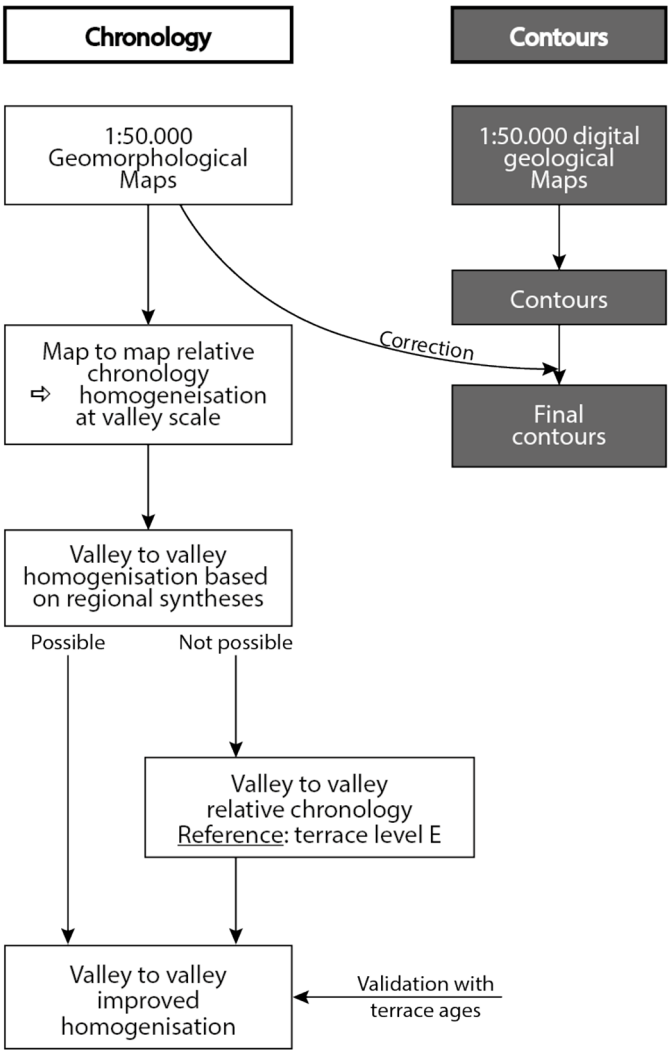


**Fig. 2.** Schematic workflow for terrace mapping (contours) and chronology.

order starting with 'a' for the oldest terrace. The terrace layouts (polygons) were taken from the digital geological map (MAGNA 50 – Mapa Geológico de España a escala 1:50 000 (2 Serie) with shapefiles, IGME; http://info.igme.es/cartografiadigital/geologica/Magna50.aspx) when the contour on the geomorphological map corresponded to the boundaries on the digital geological map (Fig. 2). When the difference between the two was judged to be too large, we manually retraced the contour of the terrace as drawn on the geomorphological map. In the rare case of disagreement from one map to another for a single valley, we chose to join or instead distinguish between entities. These geomorphological maps cover only ~20% of the basin, but most of the main valleys east of Zaragoza. In the areas not covered, we relied on the geological map and manual contouring of flat areas from the shaded DEM (MDT25 dataset from IGN) and derived slope map (Fig. 2).

The mapping of terraces has been improved by comparison with published works on the terraces of the studied valleys (*e.g.* Benito *et al.*, 2000; Stange *et al.*, 2013b; Lewis *et al.*, 2017), as well as broader syntheses from which we georeferenced the main synthesis maps (*e.g.* Alberto *et al.*, 1983; Benito *et al.*, 2000; Calle *et al.*, 2013) (Fig. 2).

This work of detailed mapping focused only on the highest terraces. We did not include any terrace in the immediate vicinity of the active stream, either geographically or in terms of elevation (< 50 m difference in elevation). Based on geological and geomorphological maps and published works (*e.g.* Lewis *et al.*, 2017), we have verified that *a priori* all the terraces older than 300–400 ka were mapped. This work resulted in more than 500 polygons, with ~250 of them being associated with a terrace level identified in the published geomorphological map or identified in a publication.

The second part of the work was to correlate the sequences of terraces. For the multiple tributaries of the Segre to the east, this work has been facilitated by the number of previously published works and existing geomorphological maps, although without any real homogenization for terrace labels (see Stange *et al.*, 2013a). Similarly, the sequence of the Gállego is well defined (Benito *et al.*, 1998, 2000). We correlate these two areas based on the mapping by Alberto *et al.* (1983) of the high terraces and the one by Mensua and Ibañez (1977) of the terraces and glacis in a large area around Zaragoza. For the Aragón and Ebro valleys, the sequences of terraces are far from the Segre/Gállego area. Despite this difficulty, we established a correlation which is first based on the lower sequence, in particular the level E, a large ubiquitous level that can be found in every valley of the Ebro Basin. This correlation is then refined on the basis of differences in altitude between the terraces (*e.g.* Julián Andrés and Chueca Cía, 1998), degrees of preservation, and an attempt of correlation by Bomer (1979), who correlated the topmost surfaces of the Segre and the Aragón valleys based on their geomorphological position and the presence of highly cemented conglomerates.

At the end of this work, certain ambiguities remained. Ultimately, to resolve these ambiguities, we have used the ages and magnetic polarities published in the literature as well as the new age constraints presented below (Fig. 2). The latter adjustments are proved to be minor, indicating our homogenisation procedure is quite robust. A few remaining mismatches reveal a potential error limited to a difference of one level. Differences in terrace level recognition also occur between our map and one of the published ones, or between two different publications (for example between the maps from Mensua and Ibañez, 1977 and from Alberto *et al.*, 1983). Following our terrace mapping workflow, we labeled each terrace level using capital letters, similar to the convention used on geomorphological maps and deliberately different from the labels used in publications, which are different for each river studied. The shapefile is available at https://doi.org/10.5281/zenodo.4721256.

### 3.2 Cosmogenic nuclide dating methods used (depth profiles and P-PINI)

*In-situ* cosmogenic nuclides are produced within the Earth's surface material through nuclear reactions (mostly spallation but also muonic capture) promoted by cosmic rays. Spallation processes occur within a couple of meters below the Earth's surface (*e.g.*, Lal, 1991; Gosse and Phillips 2001).

The concentration of *in situ*-produced (*i.e.*, produced within the crystal lattice) reflects the time the mineral spent in the production zone (c.a. from surface to few upper meters below surface). They have been extensively used for dating alluvial surfaces, assuming that both the initial mineral concentration at deposition time (thereafter called inheritance) and the denudation rate of the alluvial terrace are negligible (*e.g.*, Bierman *et al.*, 1995; Brown *et al.*, 1998; Regard *et al.*, 2005). For old terraces (> 300 ka), surface reworking may be quite significant. To overcome this problem and avoid inheritance effects, it is advisable to analyze the depth profiles of cosmogenic nuclide concentration (*e.g.*, Anderson *et al.*, 1996; Repka *et al.*, 1997; Ritz *et al.*, 2003; Hidy *et al.*, 2010), although this cannot allow to date terraces much older than 500 ka. For longer timescales, cosmogenic nuclides can be used by pairs. The analysis is very different in this case: the two cosmogenic isotopes are produced in a similar fashion in the same mineral during his life nearby the Earth's surface, allowing the knowledge of their initial concentration ratio. Then, the mineral is buried far from the surface, where cosmogenic nuclide production is negligible. Thus, the concentration ratio evolves following the various disintegration rates of the two cosmogenic nuclides. This method is called burial method (Balco and Shuster, 2009). It may be modified to take into account the production after the mineral has been buried, which has been popularized under the name of isochron method (Balco and Rovey, 2008). This method allows dating alluvial terraces up to a couple of million years (*e.g.*, Balco and Shuster, 2009; Jungers and Heimsath, 2016).

In this paper, we report new chronological constraints obtained with various cosmogenic nuclide techniques: exposure depth profiles, simple burial and P-PINI, which is an adaptation of the isochron burial method.

### 3.2.1 Basic systematics

The basics of cosmogenic nuclide systematics can be found in Gosse and Phillips (2001) and Dunai (2010). We sum up in the following the most important information. Cosmogenic nuclides are produced at Earth's surface by secondary cosmic rays (neutrons muons). Cosmic rays are quickly absorbed at depth, so that the production rate exponentially decreases against the mass of overlying material: $P(z) = P_0 e^{\rho z/\Lambda_i}$, where $P_0$ is the surface production rate (atom.g$^{-1}$.yr$^{-1}$), ρ the density (g.cm$^{-3}$), and Λ (g.cm$^{-2}$) corresponds to the attenuation length of cosmic-ray particles. Production accounts for three types of secondary cosmic rays: neutrons, slow muons and fast muons (thereafter corresponding to i = 1, 2 and 3, respectively). At an alluvial surface, the concentration C in cosmogenic nuclide depends on the age of the alluvial surface (t), its erosion rate (ε) and the initial cosmogenic nuclide content, often called inheritance (H), and the decay constant (λ):

$$C(t) = He^{-\lambda t} + \sum_i \frac{P_0 e^{\rho t/\Lambda_i}}{\lambda + \rho/\Lambda_i}\left(1 - e^{-(\lambda + \rho/\Lambda_i)t}\right).$$

If t and ε are unique for a single terrace, H varies for each sample. To determine the most probable (t, ε) pair, depth profiles are often used. Numerical processing of concentration *vs.* depth data is not straightforward and numerical procedures have been proposed, in particular, the one we used, developed by Hidy *et al.* (2010). They explore (t, ε) pairs and select the most probable ones by minimizing the difference between the observed and modelled concentrations.

Input parameters in the program provided by Hidy *et al.* (2010) are a density of 2 to 2.4 g.cm$^{-3}$, a neutron attenuation length of 160 ± 10 g.cm$^{-2}$ and a minimum number of profiles tested of 100 000. Other site-dependent input parameters were fixed after a few iterations to encompass all the range of the likely values. They are the explored age range, the maximum erosion rate, an erosion threshold. We also set the maximum inheritance to a value close to the minimum measured concentration.

Different cosmogenic nuclides can be used. For quartz-rich lithologies, the most convenient one is $^{10}$Be. Interestingly, $^{26}$Al can be also used. $^{10}$Be and $^{26}$Al are produced proportionally; the radioactive decay of $^{26}$Al being is approximately twice as fast as the $^{10}$Be (half-lives of 0.705 and 1.387 Ma, respectively). Consequently, the concentrations of surface samples in $^{10}$Be and $^{26}$Al are linked (their ratio R is ~6.6 if their source area denudation rate is not too slow). If buried, it is possible to record the burial time by recording the evolution of the ratio in the two nuclides, following their disintegration. The burial must be at high depth, far below the surface, where there is no more cosmogenic nuclide produced. This holds true for depth > 10 m. On the contrary, it is possible that production during burial is not negligible in alluvial sequences, thus the burial duration is a minimum estimate. It is possible to correct for this post-burial production by comparing the concentration in cosmogenic nuclide of various rocks sampled at a similar depth, following a method called isochron (*e.g.*, Balco and Rovey, 2008; Jungers and Heimsath, 2016). P-PINI (Particle Pathway Inversion of Nuclide Inventories) is an adapted isochron method that has been recently setup to account for complex pre-burial histories (Knudsen *et al.*, 2020). The P-PINI method applies a Monte Carlo source-to-sink model approach, in which a large range of possible exposure and erosion histories are simulated for both the source and sink areas. For the source area, this involves highly complex exposure histories and abrupt erosion events associated with the presence of ice covers. The source model thus includes three episodes of ice cover with durations ranging from 2–100 ka for the two former ones and 2–10 ka for the latter one. These ice-covered periods are characterized by a complete halt in the production of cosmogenic nuclides, and a stochastic erosion event with an erosion depth randomly selected from the range 1–10 m. Periods with no ice cover are characterized by the production of cosmogenic nuclides with a range of production rates that corresponds to the elevation range of the estimated source area. The ice-free periods are accompanied by uniform and continuous erosion with rates randomly selected from the range 1–1000 m/Ma. Each simulation of the exposure and erosion history in the source area produces a ($^{26}$Al,$^{10}$Be) nuclide pair that is used as input for the sink model. This model simulates a large range of possible burial ages, assuming that the sediments were not covered by ice after deposition and that they experienced continuous erosion with rates in the range 1–500 m/Ma throughout the burial period. The production rate in the sink model corresponds to the location and elevation of the study site after correction for the sampling depth. Altogether, the combined P-PINI model approach includes $1 \times 10^7$ simulations for each study site, and

a method known as rejection sampling is used to accept simulations that yield $^{10}$Be and $^{26}$Al concentrations that agree with measured concentrations. P-PINI includes the production of $^{10}$Be and $^{26}$Al associated with spallation, negative muon capture, and fast muons. A full in-depth description of the P-PINI model approach can be found in Knudsen *et al.* (2020).

### 3.2.2 Sampling sites

#### *3.2.2.1 Segre terraces*

The highest Segre river terrace is characterized by a large, ~30 km long pedimentation surface pediment striking NNW–SSE made of three distinct sub-levels, lying on the interfluve between the Noguera Ribagorzana and Cinca rivers (Bomer, 1979; Lucha *et al.*, 2012; Stange *et al.*, 2013a, 2013b). This set of surfaces is limited to the north, by the South Pyrenean Frontal Thrust (SPFT), close to the upstream valley of the Noguera Ribagorzana river. The highest Segre river terrace levels the Barbastro-Balaguer anticline, which outlines the SPFT (Lucha *et al.*, 2012). The organization of terrace remnants suggests an eastward shift of the Noguera Ribagorzana during deposition.

From these three alluvial surfaces, the level Qt0a (B in our terminology, see thereafter), where TSEG2 has been collected (0.573069°E, 41.70244°N, 357 m; Fig. 3), is the highest, ~160 m above the present-day Noguera Ribagorzana river. It consists in ~10 m thick of gravels deposited on top of Oligocene strata, with intercalation of sandy channels, topped by a very thin soil layer (< 10 cm). Although the top surface is flat, it is slightly dipping towards the valley indicating lateral erosion on the edges. We collected 6 samples along a depth profile from 15 to 380 cm from the surface (TSEG2, Fig. 3). We choose a sampling site with a relatively flat top to minimize post-deposition erosion, on an ancient quarry site west of the locality of Rossello.

We also sampled (TSEG1) the lowest of these uppermost levels, Terrace Qt1 (D in our terminology). This terrace is situated at ~115 m above the present-day active channel of the Noguera Ribagorzana river. It consists of polygenic imbricated conglomerates overlying Oligocene strata. The top of this section (from 0 to ~30 cm) is cemented by a calcrete as mentioned by Bomer (1979). TSEG1 (0.551336°E, 41.83316°N, 389 m) consists in 7 samples along a depth profile from 15 to 300 cm from the surface (Fig. 3). The sampling site, south to the Alfarras locality, is a small ancient quarry with no evidence of important surface erosion.

#### *3.2.2.2 Alcanadre terrace*

Sample TALC1 (−0.034394°E, 41.908655°N, 486 m) comes from an upper terrace level that forms the divide between the Alcanadre and Cinca rivers (Terrace Qt1 of Calle *et al.*, 2013; Duval *et al.*, 2015). This large terrace (~15 km long; B terrace level, see the following) is gently sloping southward (0.5%). Its elevation above the modern Alcanadre river decreases from 200 m to the North to 160 m to the south. At the sampling place, to the SW of Peralta de Alcofea, the top of the terrace is at 176 m above the current river. Samples come from a thick (> 10 m) succession of conglomerates with well-rounded gravels and pebbles in a sandy matrix and occasional large cross-beddings and sand lenses (Fig. 3). The upper part shows the development of thick soil (~3 m) with massive calcrete. Sample TALC1 consists of quartz pebbles and sand taken at depth of 8.50 m below the top of the terrace. Paleomagnetic data of Calle *et al.* (2013) indicate normal magnetic polarity near the base of the succession (at depth of ~10 m) but normal magnetic polarity above. ESR data of Duval *et al.* (2015) give ages of 1606 ± 187 and 1269 ± 157 ka for a sample at 14 m depth (sample ALC1202) and 1504 ± 229 and 1282 ± 139 ka for a sample from the upper part (depth of 4 m) of the sequence (sample ALC1201). Duval *et al.* (2015) consider that the most reliable age of this terrace is 1276 ± 104 ka.

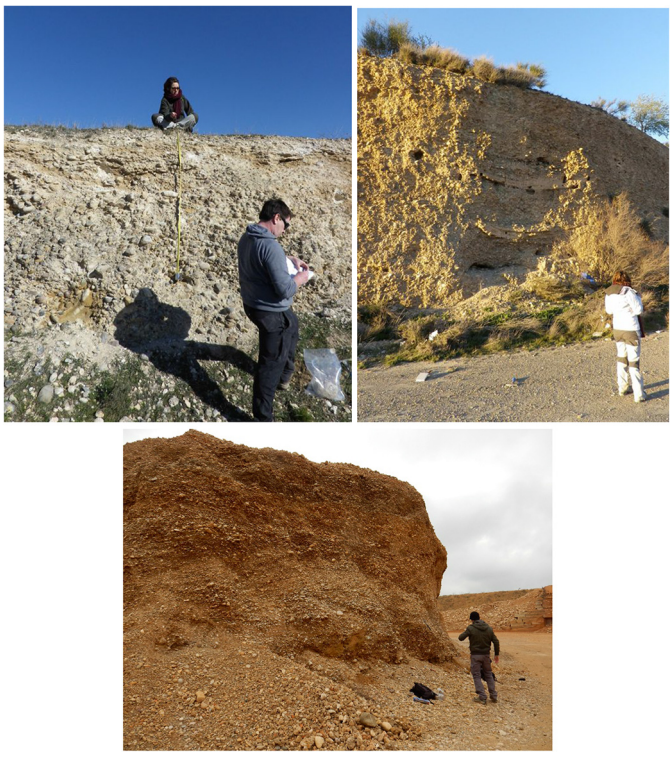

**Fig. 3.** TSEG1 (0.551336°E, 41.83316°N, 389 m, top left), TSEG2 (0.573069°E, 41.70244°N, 357 m, top right), and TALC1 (−0.034394°E, 41.908655°N, 486 m) outcrops.

#### *3.2.2.3 Aragón terrace*

The highest Aragón river terrace forms a ~25 km-long pedimentation surface (T1), slightly dipping (slope ca. 0.3%) toward the Ebro river to the south. This terrace T1 surface splits into four remnant pieces from north to south and is situated ~140 m above the Aragón river. Lower T2 to T7 terrace levels are deeply entrenched in the Aragón valley contrary to T1.

Two samples have been collected on this surface (A terrace level, see the following). The first sampling site (TARA0, −1.60158°E, 42.19839°N, 395 m) is located on the southernmost remnant and corresponds to a quarry, to the NNW of the Arguedas locality. It is characterized by >20 m of gravels with intercalations of sandy channels. The top (> 1 m) appears highly cemented by calcrete. We collected five samples from rounded quartz pebbles to sand for burial dating, at ~20 m

depth (TARA0, Fig. 4). The second sampling site (TARA2, −1.419875°E, 42.38064°N, 466 m) is located on the northernmost remnant, on an ancient quarry, NE of the locality of Carcastillo. The top is highly cemented by calcrete, up to ~ 1 m depth. We collected 5 pebbles of sandstone and quartz at ~ 9 m depth for burial dating (TARA2, Fig. 4).

#### 3.2.2.4 Ebro terrace

The highest preserved terrace record of the Ebro river (T1), located between Logroño to the west and Calahorra to the east, is largely affected by erosion and shows important alteration and soil development. Terrace T1 is situated at ~ 200 m above the active Ebro channel (likely B terrace level, see the following). We collected 5 pebbles of quartz (TEBR2, −2.207328°E, 42.40442°N, 504 m, Fig. 4) at ~ 10 m depth for burial dating.

#### 3.2.2.5 Najerilla terrace

The Najerilla river is a tributary of the Ebro whose headwaters are located in the Iberian Chain. The highest terrace record in the vicinity of the Najerilla river corresponds to a staircase of four distinct terraces, characterized by a slightly NW dipping (slope ca. ~ 0.6%). The lowest level (T4) is the most extensive (~ 10 km large), the highest (T1) only show a limited remnant (~ 700 m large).

Terrace T1 is situated at ~ 245 m above the Najerilla active channel (*a priori* corresponding to A or B terrace level, see the following). Field observations indicate important surface erosion on the top of the terrace and soil development. We collected 5 samples of quartz and sandstone pebbles at ~ 7.5 m depth for burial dating (TOJA1, −2.775386°E, 42.461922°N, 701 m).

### 3.2.3 Laboratory analyses and age calculations

All the samples were processed at CEREGE following standard procedures (*cf.* Braucher *et al.*, 2015). They were measured at ASTER AMS (Tab. 1; Arnold *et al.*, 2010).

(a)

(b)

**Fig. 4.** TARA0 (A, −1.60158°E, 42.19839°N, 395 m) and TARA2 (B, −1.419875°E, 42.38064°N, 466 m) sampling sites.

## 4 Results

Mapping and homogenization of terrace sequences resulted in the morphological maps presented in Figures 5 and 6. The mapping is comprehensive for the highest levels from A to D. The terraces corresponding to level E have been mapped where they represent an important reference in the establishment of the sequence (*e.g.* along the Gállego or Aragón rivers, Figs. 5 and 6).

We recognize the highest, oldest terrace level, labelled "A", in the upper Ebro and Aragón valleys (Figs. 5 and 6). This level A constitutes probably the uppermost terrace remnants, sparsely remaining along the Ebro valley, lying more than 200 m above the current river (Fig. 7a). This level is deformed near the confluence between the Aragón and Ebro rivers, suggesting it is much older than the subsequent ones. "B", "C", and "D" levels have been defined following the three levels identified on the interfluve between the Noguera Ribagorçana and the Cinca rivers (Alberto *et al.*, 1983; Stange *et al.*, 2013a; Lewis *et al.*, 2017) (Figs. 5 and 6). Remnants of last level "D" are not parallel to the current river network and lie generally ~ 100 m over the current rivers (Fig. 7). "E" is a usually extensive level, usually lying 40–60 m above current river courses (Figs. 5 and 6); it corresponds to Qt4 of Lewis *et al.* (2017).

### 4.1 Dating results

For TSEG1, eight samples have been measured (Tab. 1 and Fig. 8). Two $^{10}$Be Concentrations cannot be measured (Tab. 1). The $^{26}$Al concentration of the point at 50 cm depth is probably erroneous (it is 3 to 6 times less than the neighboring samples, Tab. 1) and has been discarded. $^{10}$Be and $^{26}$Al profiles lead to best age estimates of 693 ka (most probable age range 523–1095 ka), and 422 ka (most probable age range 400–971 ka), respectively (Tab. 2). The profiles indicate that erosion rates are most probably less than 1 m/Ma, and certainly less than 2.1 m/Ma (Tab. 2). The overlap of $^{10}$Be and $^{26}$Al results defines a common range of 523–971 ka for TSEG1 (Figs. 5 and 6).

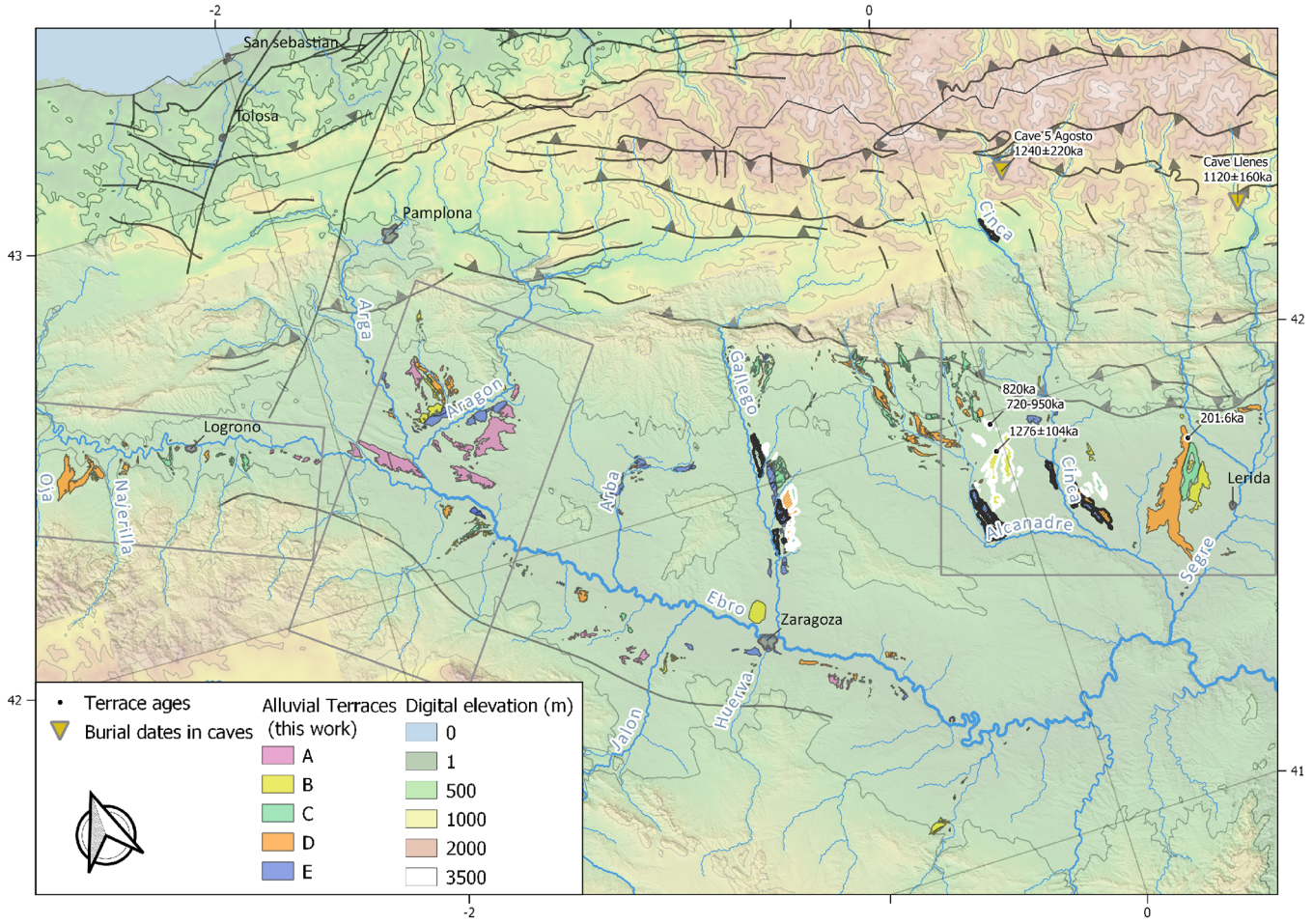


**Fig. 5.** Map of the uppermost terrace record (levels A–E) in the Ebro Basin. The background corresponds to elevation. The topmost terraces are shown with the available dates for them, both from the literature and from this study. Two burial ages from Genti (2015) are mentioned: they may be related to these topmost terraces. Rectangles figure zooms of this map; they can be found in Figure 6. The produced shapefile is freely available on Zenodo (https://doi.org/10.5281/zenodo.4721256).

Six TSEG2 samples have been measured (Fig. 8). $^{10}$Be and $^{26}$Al profiles lead to best age estimates of 532 ka (most probable age range 489–1961 ka), and, 435 ka (most probable age range 374–1104 ka), respectively (Tab. 2). Erosion rates are most probably less than 1.8 m/Ma (Tab. 2). The overlap of $^{10}$Be and $^{26}$Al results defines a common range of 489–1104 ka for TSEG2 (Figs. 5 and 6).

For TARA0, P-PINI indicates a best terrace age of 4731 ± 1447 ka (Tab. 3). For TARA2, P-PINI computed 2215 ± 778 ka (Tab. 3). For TEBR2, TOJA1, and TALC1, P-PINI indicates ages of, respectively, 1034 ± 275 ka, 957 ± 161 ka, and 5016 ± 1702 ka (Tab. 3 and Figs. 5 and 6). The large uncertainty for TALC1 and TARA2 comes from a low (insufficient) number of samples and that the concentrations are too similar to be well constrained by the P-PINI or Isochron method (Balco and Rovey, 2008).

### 4.2 Unified terrace chronology

Previously, we have presented our relative terrace chronology, leading to terrace levels labelled in alphabetical order starting with A. We now analyze the absolute chronology.

Previous works mainly focused in the eastern part of the basin. In the Segre catchment, study sites from B and C levels provided inverse magnetic polarity while the magnetic polarity is normal for sites from D (Fig. 9) (Calle *et al.*, 2013; Lewis *et al.*, 2017). ESR dates proposed are 1276 ± 104 ka and 817 ± 68 ka (Duval *et al.*, 2015), for terraces mapped as B and C, respectively (Fig. 9). Our P-PINI burial age for B at TALC1 is 5016 ± 1702 ka appears erroneous maybe because it is poorly constrained, probably because of too little data. Our dates from cosmogenic depth profiles are 489–1104 ka for B (TSEG2) and 523–971 ka for D (TSEG1, Figs. 6 and 9). Besides, Lewis *et al.* (2017) proposed an age of 401 ± 117 ka for the next terrace level (E, Fig. 9).

Towards the west, around the Aragón valley, even if it is tempting to correlate the topmost terrace of Bomer (1979) with the B level, the topmost terrace is likely to be much older, as emphasized by the old cosmogenic nuclide ages (> 2 Ma) found for TARA0, TARA2 upstream from the confluence from the Aragón and Ebro rivers (Figs. 5, 6 and 9). This antiquity is further confirmed by the deformation of this terrace level, whereas the lower levels, including the well-developed E level in the area, are not deformed (see Casas *et al.*, 1994 and the corresponding 1:50 000 geological map).

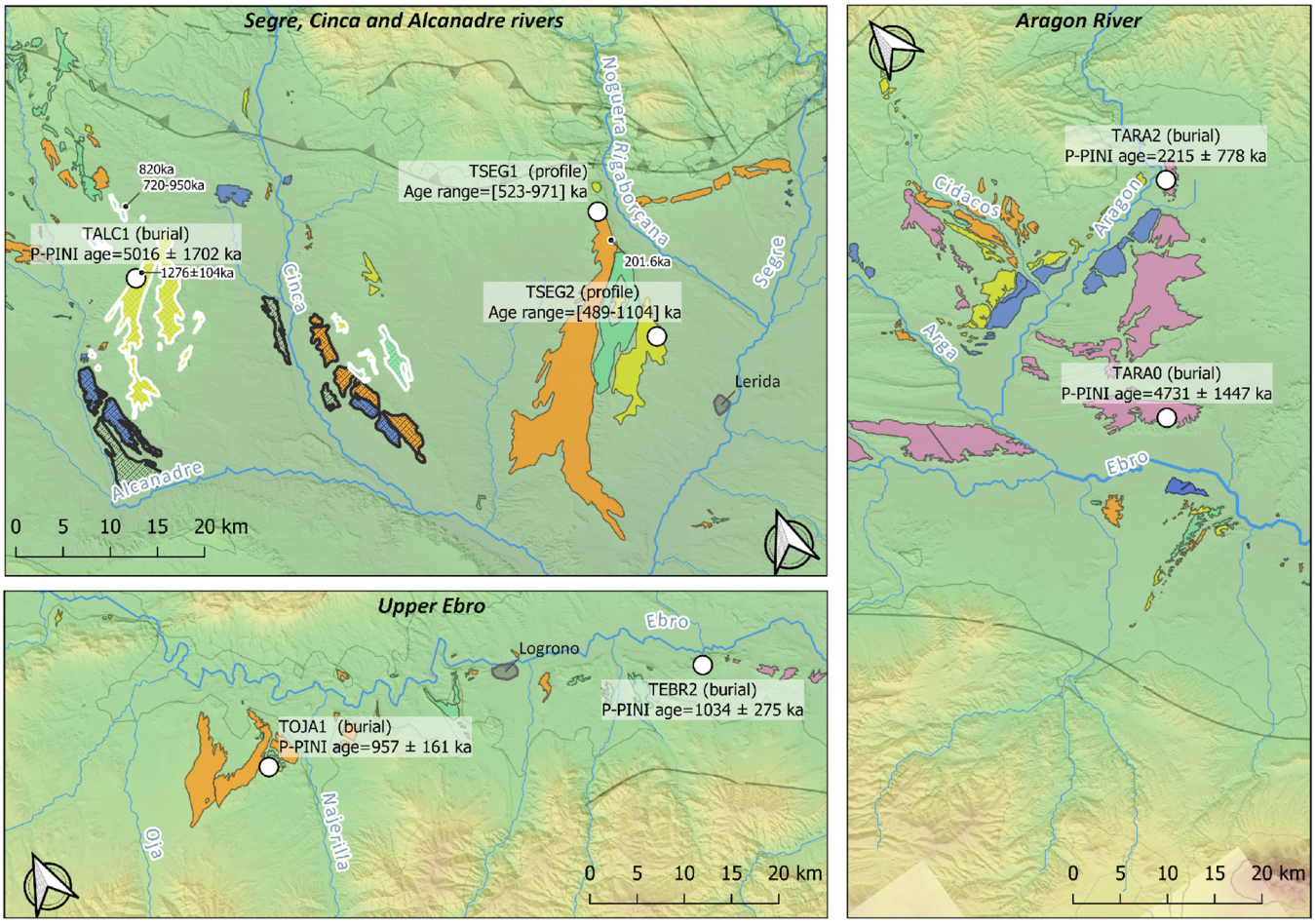


**Fig. 6.** Zooms of Figure 5 for places of interest discussed in this work. Same legend as Figure 5.

The A level was not previously dated. It corresponds to two sites from the present study (TARA0 and TARA2). The P-PINI dates for these two sites are quite different but both agree on a fairly old age. None of the dates are very reliable due to the low number of data. Since we cannot choose between the two, we adopt the mean age of ~2.8 ± 0.7 Ma (Tab. 4). We note, however, that this age represents well the samples TARA0-B, TARA0-D, TARA2-C and TARA2-D (Supplementary Material, Figs. S10 and S13). The B level was deposited with inverse magnetic polarity (Calle *et al.*, 2013; Lewis *et al.*, 2017), and dated at ~ 1.3 Ma (Duval *et al.*, 2017). TSEG2, sampled from this level, yields an age of 489–1104 ka, by a cosmogenic profile method (Fig. 9). Also, TOJA1 (960 ± 160 ka), in the upper reaches of the Ebro main valley, could correspond to this level. We had some doubt regarding which terrace level, A or B, TEBR2 belongs to. Its P-PINI age of 1.03 ± 0.27 Ma clearly falls in the range of the level B (Tab. 4). Consequently, and considering B is older than C (see below), we regard an age of 1.15 ± 0.15 Ma to be likely for this level B (Tab. 4). The age of C, the next level, is constrained by an inverse magnetic polarity (Lewis *et al.*, 2017), and one ESR estimate of ~ 0.8 Ma (Duval *et al.*, 2017). Its likely age is 850 ± 70 ka after our analysis (Fig. 9 and Tab. 4). The terrace level D mostly displays a normal magnetic polarity (Calle *et al.*, 2013; Lewis *et al.*, 2017). We estimate an age of 523 to 971 ka (TSEG1) from our cosmogenic depth profile that is much older than the estimate by Stange *et al.* (2013a). Together with the C and E terrace dates, which must be older and younger, respectively, we propose an age of ~ 650 ± 130 ka for this D level (Fig. 9 and Tab. 4). Finally, terrace E has been dated to be 401 ± 117 ka (Lewis *et al.*, 2017) (Fig. 9). We summarize the absolute age constraints on Table 4: we estimate ages for terraces A, B, C, D, E to be 2.8 ± 0.7 Ma, 1.15 ± 0.15 Ma, 850 ± 70 ka, 650 ± 130 ka and 400 ± 120 ka, respectively (Fig. 9 and Tab. 4).

## 5 Discussion

The youngest sediments of the endorheic stage preserved in the Ebro Basin are late Miocene (see Section 2.2) lacustrine and fluvial deposits (Pérez-Rivarés *et al.*, 2002; García-Castellanos *et al.*, 2003; Pérez-Rivarés *et al.*, 2004; García-Castellanos, 2006; Larrasoaña *et al.*, 2006; Vázquez-Urbez *et al.*, 2013; Calvet *et al.*, 2020). They are observed 500 m above the Ebro river course, and have possibly been covered by younger sediments now eroded (García-Castellanos and Larrasoaña, 2015). The subsequent erosion of the Ebro basin was limited and affected mostly the Miocene deposits that are currently preserved in the form of alluvial deposits but also pediments. Plio-Pleistocene alluvial remnants are mostly

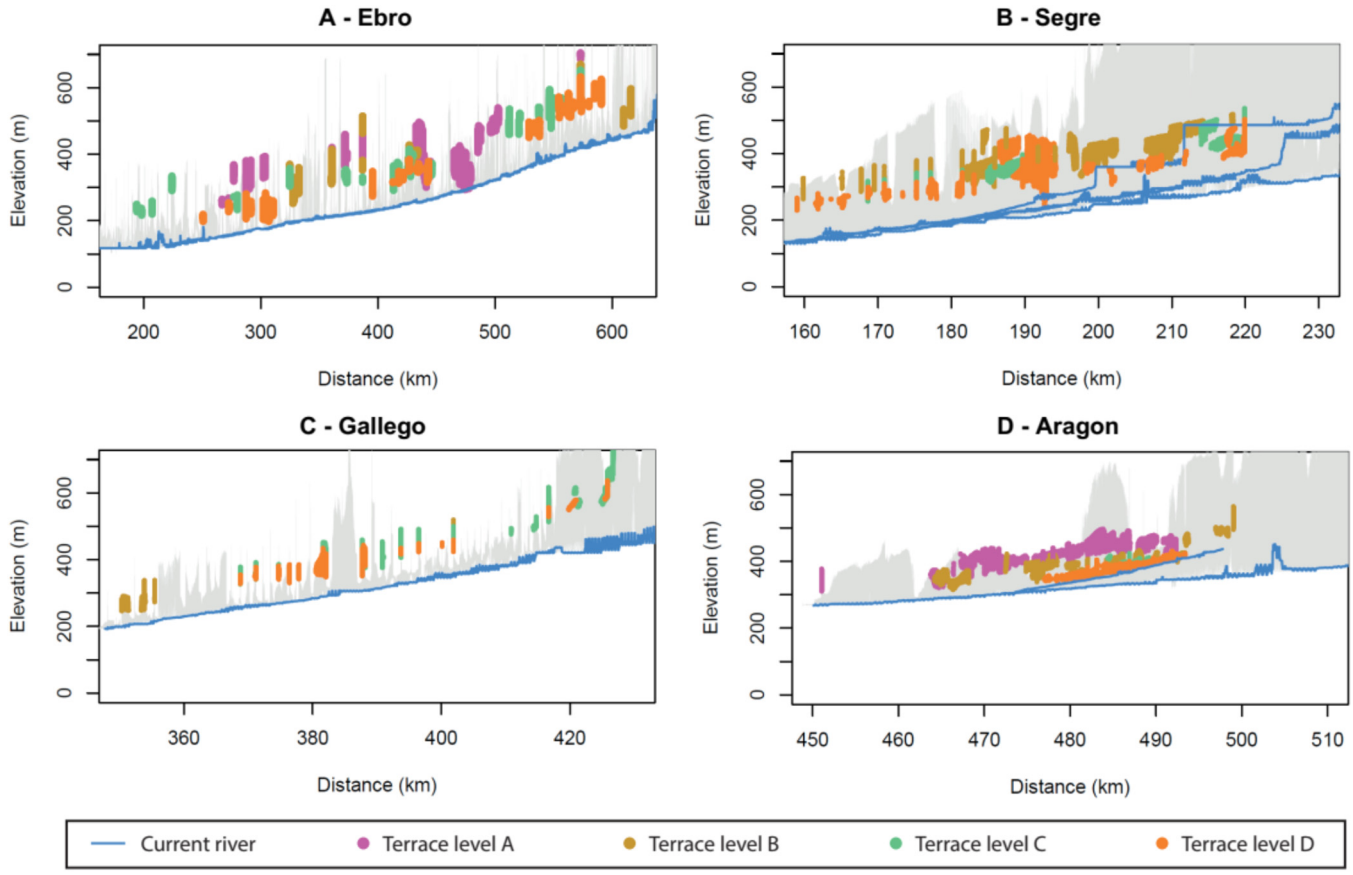


**Fig. 7.** Profiles elevation *vs.* distance for the main river systems and their terraces. Grey: elevation in 10 km-large buffer (area within 10 km of the river) around the river trace (*cf.* Fig. 1). The topmost terraces are shown as color dots. The color code is a function of the unified sequence defined in the results part (*cf.* Fig. 5). The panels stand for: (A) the Ebro main stream, (B) the Segre and tributaries, (C) the Gállego valley and (D) the Aragón and Cidacos valleys. The x-axis is the distance to the Ebro mouth.

terraces found along (and parallel to) the main rivers in valleys within the basin. Some of these remnants are lying on interfluve crests between the main valleys. Among them, good examples are represented by terraces between the Noguera Ribagorçana and the Cinca valleys (levels B, C, and D). These uppermost terraces argue for a mobile fluvial network while the lowermost ones reflect river entrenchment without significant lateral mobility. This change in fluvial behavior seems to have occurred at the time of deposition of terrace level D, shortly after the Brunhes-Matuyama transition at 780 ka (Fig. 9). This agrees with the change in fluvial style at the Mid-Pleistocene Transition proposed by Sancho *et al.* (2016).

### 5.1 Terrace chronology

The proposed chronology for terraces A, B, C, D, E is 2.8 ± 0.7 Ma, 1.15 ± 0.15 Ma, 850 ± 70 ka, 650 ± 130 ka and 400 ± 120 ka, respectively (Fig. 9). These dates are the result of a compilation of ages obtained with various methods (Tab. 4): ESR, paleomagnetism, cosmogenic nuclide depth profiles, and cosmogenic nuclide burial ages from the isotope pair ($^{10}$Be, $^{26}$Al) (in caves and in terraces through P-PINI inversion). The number and quality of data for each level of terrace are variable. For example, paleomagnetism only indicates if the terrace level is younger or older than the Brunhes-Matuyama transition (780 ka). Also, after our own experience, cosmogenic nuclide depth profiles are not accurate when the ages exceed 500 ka, and can be significantly altered by terrace post-abandonment surface evolution. For example, the ages computed from depth profiles published in Stange *et al.* (2013a) are probably underestimated (see also Delmas *et al.*, 2018; Delmas, 2019). Similarly, our own depth profiles, which do not give an unequivocal result, probably tend to underestimate the ages, possibly because of a recent acceleration of erosion. The 2.8 ± 0.7 Ma for the level A is not very good because the two estimates on the uppermost Aragón terrace largely differ (TARA0 at 4730 ± 1450 ka and TARA2: 2210 ± 780 ka). The level B benefits from a large number of dating attempts. Its P-PINI cosmogenic burial dates agree with ESR (except for TALC1) and an inverse magnetic polarity. The age suggested by our depth profile data (TSEG-2) is a bit younger than the average age of ~ 1150 ka calculated for level B but is older than the age proposed by Stange *et al.* (2013a). Level C delivered only two but overlapping pieces of information, making it reliable: an inverse magnetic polarity (Lewis *et al.*, 2009) and an ESR age of 817 ± 68 ka (Duval *et al.*, 2017). On level D, we produced a depth-profile cosmogenic age, which, despite the aforementioned caveats, and with the constraint of normal magnetic polarity, allows to restrict the range of possible ages to 650 ± 130 ka.

**Table 1.** Measured $^{10}$Be and $^{26}$Al concentrations.

| Sample | Mass Quartz g | Spike $^{9}$Be at | +/− | $N10_{Be}$ | Measured $^{10}$Be/$^{9}$Be | uncertainty measure +blank % | [$^{10}$Be] at/g | +/− | $27_{Al}$ at | +/− | N $^{26}$Al | Measured $^{26}$Al/$^{27}$Al | uncertainty measure % | [$^{26}$Al] at/g | +/− | [$^{26}$Al]/[$^{10}$Be] | +/− | Burial time ka |
|---|---|---|---|---|---|---|---|---|---|---|---|---|---|---|---|---|---|---|
| TSEG1-015 | 20.70 | 2.029E+19 | 6.040E+16 | 202 | 1.05E-12 | 8.95 | 1026 581 | 92 269 | 1.108E+18 | 1.507E+15 | 1183 | 4.86E-12 | 3.13 | 5386 443 | 168 759 | 5.25 | 0.50 | |
| TSEG1-050 | 8.99 | 2.035E+19 | 6.058E+16 | 150 | 4.84E-13 | 8.26 | 1087 814 | 90 624 | 1.116E+19 | 1.101E+17 | 95 | 8.74E-14 | 10.33 | 975 482 | 101 178 | 0.90 | 0.12 | |
| TSEG1-075 | 22.16 | 2.030E+19 | 6.044E+16 | Not measurable | | | | 1.004E+18 | 1.668E+15 | 138 | 3.41E-12 | 10.61 | 3419 316 | 362 985 | | | | |
| TSEG1-110 | 15.36 | 2.038E+19 | 6.066E+16 | 1208 | 4.62E-13 | 3.32 | 608 128 | 20 466 | 1.997E+18 | 3.046E+15 | 488 | 1.57E-12 | 5.04 | 3131 287 | 157 833 | 5.15 | 0.31 | |
| TSEG1-138 | 22.10 | 2.035E+19 | 6.057E+16 | Not measurable | | | | 2.398E+18 | 1.833E+15 | 407 | 9.19E-13 | 5.09 | 2204 089 | 112 214 | | | | |
| TSEG1-300 | 21.79 | 2.037E+19 | 6.065E+16 | 158 | 9.75E-14 | 8.05 | 87 476 | 7382 | 2.991E+18 | 3.160E+14 | 131 | 1.68E-13 | 8.81 | 500 990 | 44 155 | 5.73 | 0.70 | |
| TSEG1Enf. 1 | 5.73 | 2.030E+19 | 6.043E+16 | 17 | 2.62E-14 | 25.54 | 78 773 | 23 885 | 1.114E+19 | 2.425E+15 | 11 | 1.54E-14 | 31.41 | 171 606 | 53 895 | 2.18 | 0.95 | 2314 |
| TSEG1Enf. 2 | 20.51 | 2.034E+19 | 6.055E+16 | 20 | 1.05E-13 | 22.88 | 100 670 | 23 952 | 5.625E+18 | 2.487E+16 | 61 | 6.41E-14 | 12.86 | 360 284 | 46 346 | 3.58 | 0.97 | 1291 |
| TSEG2-016 | 20.50 | 2.039E+19 | 6.071E+16 | 1224 | 1.44E-12 | 3.25 | 1426 290 | 46 722 | 2.272E+18 | 9.221E+14 | 1174 | 2.89E-12 | 3.23 | 6567 168 | 212 433 | 4.60 | 0.21 | |
| TSEG2-040 | 18.51 | 2.036E+19 | 6.059E+16 | 767 | 7.60E-13 | 3.81 | 831 022 | 31 947 | 5.239E+18 | 1.343E+16 | 534 | 7.93E-13 | 4.48 | 4152 099 | 186 321 | 5.00 | 0.30 | |
| TSEG2-100 | 20.09 | 2.037E+19 | 6.064E+16 | 293 | 5.45E-13 | 6.30 | 548 576 | 34 870 | 7.705E+18 | 1.886E+16 | 264 | 3.11E-13 | 6.26 | 2396 931 | 150 230 | 4.37 | 0.39 | |
| TSEG2-130 | 22.28 | 2.036E+19 | 6.060E+16 | 331 | 4.74E-13 | 5.93 | 429 618 | 25 738 | 2.528E+18 | 9.145E+15 | 915 | 8.12E-13 | 3.53 | 2052 626 | 72 889 | 4.78 | 0.33 | |
| TSEG2-180 | 20.08 | 2.039E+19 | 6.069E+16 | 47 | 3.48E-13 | 15.47 | 349 487 | 54 713 | 2.406E+18 | 3.713E+15 | 229 | 5.21E-13 | 6.71 | 1253 418 | 84 116 | 3.59 | 0.61 | |
| TSEG2-380 | 20.69 | 2.034E+19 | 6.053E+16 | 45 | 2.10E-13 | 14.96 | 202 286 | 30 856 | 3.440E+18 | 1.484E+16 | 79 | 1.10E-13 | 11.51 | 378 538 | 43 589 | 1.87 | 0.36 | |
| TEBR2enf. 1A | 20.68 | 2.034E+19 | 6.055E+16 | 835 | 3.29E-13 | 3.67 | 319 513 | 11 931 | 3.197E+18 | 8.458E+15 | 248 | 3.38E-13 | 6.89 | 1079 230 | 74 443 | 3.38 | 0.26 | 1395 |
| TEBR2enf. 1B | 20.23 | 2.037E+19 | 6.062E+16 | 277 | 1.12E-13 | 6.13 | 108 276 | 6938 | 4.333E+18 | 2.008E+16 | 155 | 1.47E-13 | 8.12 | 638 458 | 51 898 | 5.90 | 0.61 | 261 |
| TEBR2enf. 1C | 21.05 | 2.035E+19 | 6.058E+16 | 308 | 1.77E-13 | 6.15 | 167 407 | 10 572 | 4.394E+18 | 4.504E+16 | 136 | 1.40E-13 | 8.65 | 613 864 | 53 489 | 3.67 | 0.39 | 1236 |
| TEBR2enf. 1D | 20.23 | 2.041E+19 | 6.077E+16 | 273 | 1.25E-13 | 6.26 | 122 053 | 7945 | 4.819E+18 | 1.666E+16 | 155 | 1.54E-13 | 9.08 | 741 854 | 67 397 | 6.08 | 0.68 | 198 |
| TEBR2enf. 1E | 21.67 | 2.039E+19 | 6.069E+16 | 396 | 1.78E-13 | 5.38 | 163 515 | 9038 | 3.997E+18 | 1.135E+16 | 100 | 1.65E-13 | 10.07 | 660 776 | 66 547 | 4.04 | 0.46 | 1037 |
| TALC1Enf. 1A | 20.45 | 2.039E+19 | 6.069E+16 | 69 | 5.49E-14 | 12.72 | 50 751 | 7005 | 2.873E+18 | 9.242E+15 | 84 | 1.01E-13 | 10.97 | 290 656 | 31 905 | 5.73 | 1.01 | 324 |
| TALC1Enf. 1B | 20.87 | 2.040E+19 | 6.074E+16 | 82 | 9.62E-14 | 11.70 | 90 181 | 11 038 | 4.102E+18 | 1.739E+16 | 25 | 5.37E-14 | 20.79 | 220 174 | 45 793 | 2.44 | 0.59 | 2079 |
| TALC1Enf. 1C | 21.60 | 2.040E+19 | 6.073E+16 | 24 | 6.84E-14 | 20.45 | 60 872 | 13 238 | 1.468E+18 | 1.276E+15 | 61 | 1.52E-13 | 15.11 | 223 414 | 33 760 | 3.67 | 0.97 | 1241 |
| TALC1Enf. 1F | 20.60 | 2.038E+19 | 6.065E+16 | 99 | 8.63E-14 | 12.36 | 81 433 | 10 584 | 4.713E+18 | 3.363E+16 | 30 | 6.53E-14 | 18.29 | 307 716 | 56 337 | 3.78 | 0.85 | 1037 |
| TOJA1Enf. 1A | 22.17 | 2.035E+19 | 6.057E+16 | 189 | 1.35E-13 | 7.38 | 119 890 | 9148 | 3.300E+18 | 5.844E+15 | 146 | 1.86E-13 | 8.36 | 613 540 | 51 284 | 5.12 | 0.58 | 553 |
| TOJA1Enf. 1B | 12.11 | 2.039E+19 | 6.068E+16 | 194 | 7.63E-14 | 7.28 | 121 779 | 9458 | 1.929E+18 | 8.640E+14 | 70 | 2.67E-13 | 13.46 | 515 189 | 69 368 | 4.23 | 0.66 | 945 |
| TOJA1Enf. 1C | 14.49 | 2.038E+19 | 6.067E+16 | 244 | 7.94E-14 | 6.52 | 106 127 | 7373 | 4.332E+18 | 1.446E+16 | 118 | 1.40E-13 | 9.28 | 606 021 | 56 266 | 5.71 | 0.66 | 328 |
| TOJA1Enf. 1D | 16.50 | 2.041E+19 | 6.076E+16 | 1205 | 3.82E-13 | 3.22 | 467 256 | 15 310 | 3.999E+18 | 4.716E+15 | 414 | 5.19E-13 | 5.05 | 2073 744 | 104 745 | 4.44 | 0.27 | 832 |
| TOJA1Enf. 1E | 18.79 | 2.043E+19 | 6.082E+16 | 132 | 1.72E-13 | 8.79 | 183 093 | 16 503 | 3.031E+18 | 2.391E+15 | 21 | 1.26E-13 | 23.75 | 381 067 | 90 495 | 2.08 | 0.53 | 2400 |
| TARA0enf. 1A | 5.97 | 2.038E+19 | 6.066E+16 | 61 | 1.64E-14 | 14.04 | 42 544 | 8334 | 3.711E+18 | 1.053E+16 | 11 | 3.43E-14 | 30.17 | 127 392 | 38 440 | 2.99 | 1.08 | 1662 |
| TARA0enf. 1B | 23.00 | 2.047E+19 | 6.093E+16 | 108 | 6.30E-14 | 10.89 | 52 499 | 6146 | 1.951E+18 | 4.376E+15 | 71 | 7.98E-14 | 11.92 | 155 627 | 18 561 | 2.96 | 0.50 | 1682 |
| TARA0enf. 1D | 7.39 | 2.062E+19 | 6.137E+16 | 32 | 2.92E-14 | 17.72 | 70 297 | 14 592 | 6.034E+18 | 5.085E+15 | 17 | 2.68E-14 | 24.28 | 161 699 | 39 263 | 2.30 | 0.73 | 2203 |
| TARA2enf. 1A | 22.07 | 2.045E+19 | 6.088E+16 | 120 | 1.22E-13 | 10.58 | 109 834 | 12 039 | 4.077E+18 | 2.841E+16 | 57 | 1.21E-13 | 13.73 | 493 236 | 67 810 | 4.49 | 0.79 | 822 |
| TARA2enf. 1C | 8.53 | 2.038E+19 | 6.068E+16 | 34 | 3.69E-14 | 17.19 | 78 582 | 15 264 | 5.619E+18 | 3.179E+15 | 16 | 4.10E-14 | 25.03 | 230 377 | 57 656 | 2.93 | 0.93 | 1703 |
| TARA2enf. 1D | 4.11 | 2.044E+19 | 6.086E+16 | 67 | 3.22E-14 | 12.28 | 140 468 | 20 071 | 9.166E+18 | 8.460E+15 | 14 | 3.11E-14 | 27.75 | 285 331 | 79 194 | 2.03 | 0.63 | 2451 |
| Process blank | | 2.026E+19 | 6.032E+16 | 25 | 3.97E-15 | 20.04 | | | 2.253E+19 | 4.592E+16 | 0 | 0.00E+00 | ∞ | | | | | |

**Table 2.** Input parameters and results of cosmogenic depth profile inversions (for more details, see Supplementary Material Tab. S2 and Fig. S2).

| | TSEG1 | | TSEG2 | |
|---|---|---|---|---|
| | $^{10}$Be | $^{26}$Al | $^{10}$Be | $^{26}$Al |
| ***Inputs*** | | | | |
| Age range (ka) | 400–1400 | | 200–2000 | |
| Erosion rate max (m/Ma) | 5 | | 2.5 | |
| Erosion threshold (m) | 2 | | 4 | |
| Ineritance max (at/g) | 80 000 | 360 000 | 250 000 | 400 000 |
| ***Results*** | | | | |
| Best age (ka) | 693 | 422 | 532 | 435 |
| Age range (ka) | 523–1095 | 400–971 | 489–1961 | 374–1104 |
| Common age range (ka) | 523–971 | | 489–1104 | |
| Erosion rate max (m/Ma) | 1 | 2.1 | 1.8 | 1.6 |
| Ineritance max (at/g) | 44 000 | 300 000 | 24 000 | 300 000 |

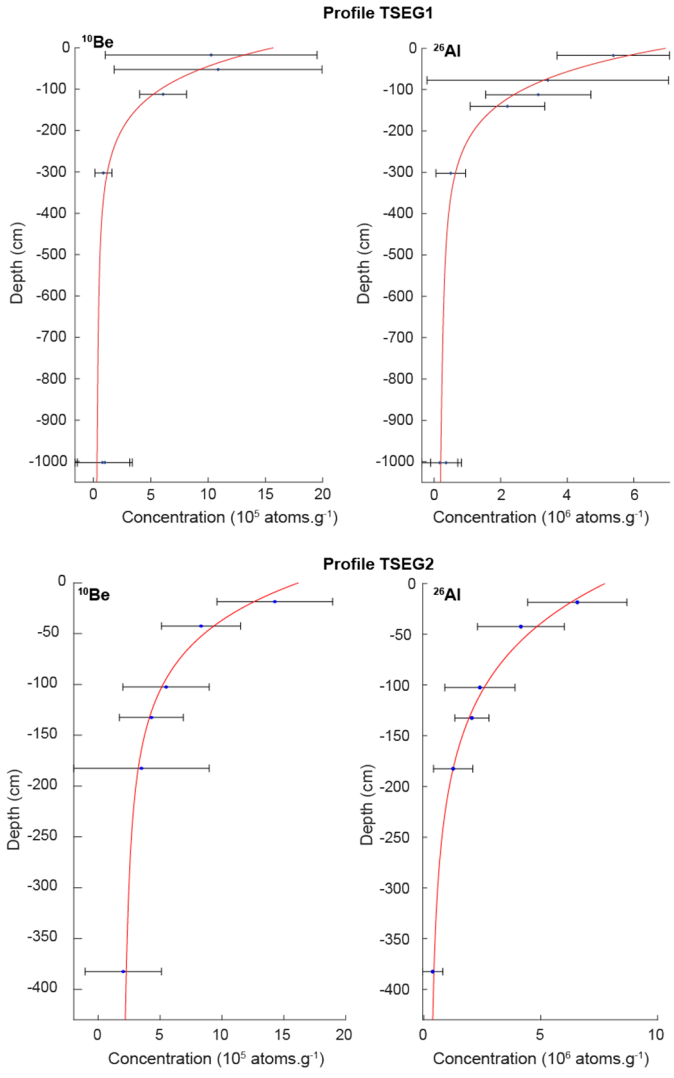


**Fig. 8.** Cosmogenic nuclide concentration profiles TSEG1 et TSEG2 (best profile).

In the nearby Arlanzon valley in the upper part of the Duero basin (location shown in Fig. 1), Moreno *et al.* (2012) used the ESR technique to date the uppermost terraces: 1140 ± 130 ka for the T3 terrace, 780 ± 120 ka and 939 ± 100 ka for the inverse polarity T4 terrace, 700 ± 100 ka, 600 ± 100 ka, and 700 ± 70 ka for T5, and 400 ± 90 ka, and 370 ± 70 ka for T8. These ages agree well with our own estimates: the Arlanzon terraces T8, T5, T4, and T3 correlate with the Ebro Basin terraces E, D, C and B respectively (*cf.* Fig. 1). Similarly, on the northern side of the Pyrenees, the uppermost Têt river terrace (T5) has provided two ESR dates at 1099 ± 179 ka and 1133 ± 159 ka (Delmas *et al.*, 2018), again contemporaneous to B. Along the Têt river, age of T4 is still debated while the T3 terrace level below has been dated with ESR technique to be ~ 400 ka (440 ± 39 ka, and 374 ± 47 ka)(Delmas *et al.*, 2018). The Têt terraces T5 and T3 should then correspond to our B and E levels, respectively, as already noted by Delmas *et al.* (2018). In the Pyrenees, some karst dates fall within the age range we propose in the Ebro basin. The Llenes cave, located ~ 100 m above the present course of the river, and dated by $^{26}$Al/$^{10}$Be burial dating to 1120 ± 160 ka (Genti, 2015), could certainly be correlated with level B (see Calvet *et al.*, 2015 and refs included for the correlation between cave systems and terraces). More doubtful is Cave 5 of Agosto which has a similar age (1240 ± 220 ka Genti, 2015), but at a much higher elevation (800 m above the present river). Finally, it appears that the chronology of the Ebro basin shares lots of similarities with adjacent areas. We conclude that the distribution of terrace ages is a regional signal, not specific to the Ebro Basin.

We observed that rivers begin to entrench around terrace levels B to D: it marks the transition from large terraces now lying on interfluves to sequences of young terraces developing parallel to the current river courses. On the basis of physical models (Bufe *et al.*, 2016; Baynes *et al.*, 2020) as well as natural systems (Bufe *et al.*, 2017), it turns out that large terraces are produced by high channel mobility, which in turn depends on water and sediment fluxes, themselves a function of climate. As already proposed by Sancho *et al.* (2016), it is tempting to relate this entrenchment to climate as it has occurred during or shortly after the Middle Pleistocene

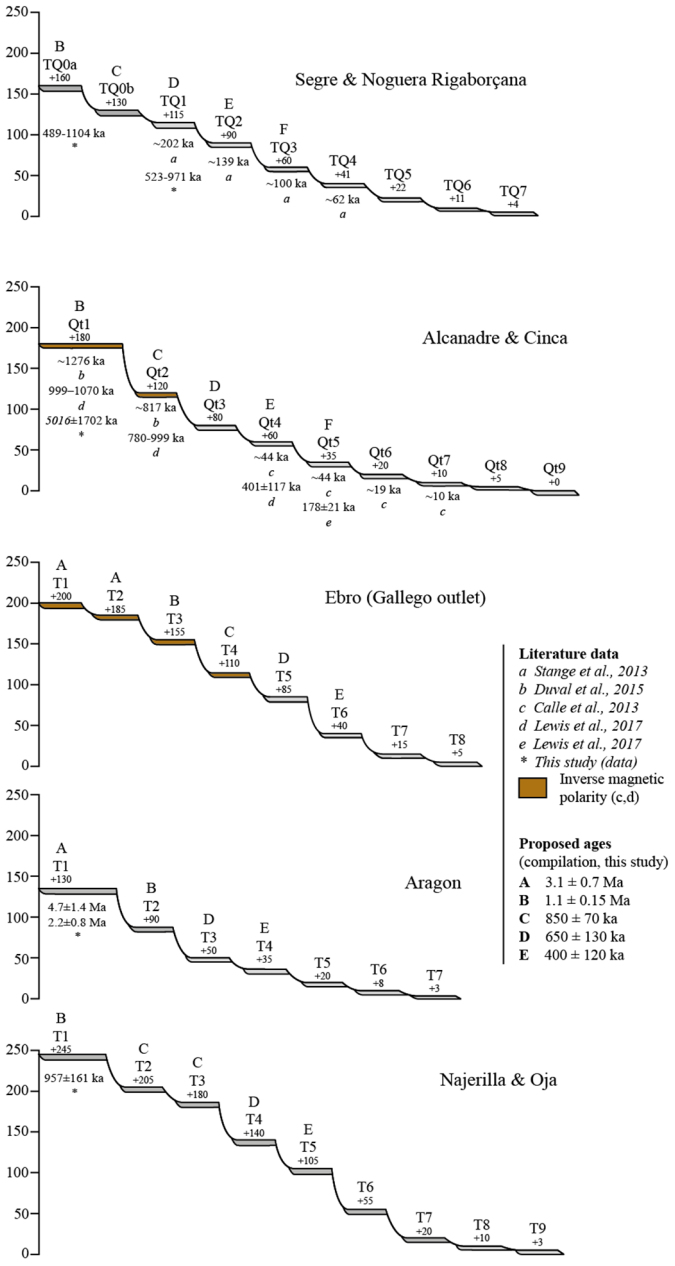


**Fig. 9.** Terrace elevation (above current river course) and labels from the literature and our homogenization scheme (A to F); maroon-colored terraces represent pre- Brunhes/Matuyama transition (780 ka), when measured. Published and new dates are indicated, as well as our proposed chronology.

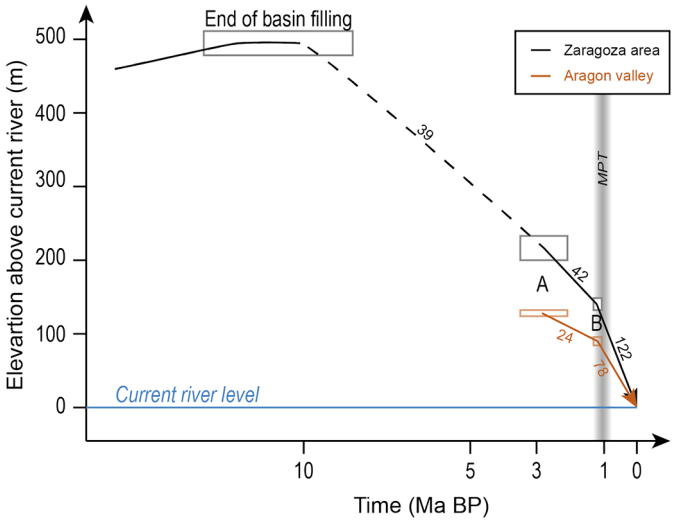


**Fig. 10.** Incision in the Ebro Basin since 10 Ma in two key areas, the Zaragoza area (black) where the end of basin infilling is recorded, and the Aragón valley (brown). Rectangles figure the constraints. Numbers represent the incision rate in m/Ma. The path for the period between 10 and 3 Ma is shown with a dashed line, which figures the possibility the current topmost strata has been buried for a while (García-Castellanos and Larrasoaña, 2015). The Zaragoza area does not show a marked change at ~3 Ma. On the contrary, both records suggest a threefold increase in incision rates after the MPT.

**Table 3.** Main burial dates from P-PINI inversion (for more information, *cf.* Supplementary Material).

| Site | P-PINI age (ka) | ± |
|---|---|---|
| TARA0 | 4731 | 1447 |
| TARA2 | 2215 | 778 |
| TEBR2 | 1034 | 275 |
| TOJA1 | 957 | 161 |
| TALC1 | 5016 | 1702 |

Transition (MPT, 1.3 to 0.7 Ma ago). Indeed, the MPT is due to dominant orbital periodicity change from 41 ka to 100 ka (Tziperman and Gildor, 2003; Lisiecki and Raymo, 2005; Siddall *et al.*, 2010). This led to an increase of climatic contrasts, triggering intense glacier fluctuations in the surrounding mountain ranges and controlling sediment discharge and river incisions, similar to what we observe in the Ebro Basin (Stange *et al.*, 2013a, 2013b; Lewis *et al.*, 2017). Our observations further suggest that before the MPT, the upper Pliocene/lower Pleistocene climate favored a mobile river network. This idea is, on the one hand, challenged by Santisteban and Schulte (2007) who claimed for a diachronous incision beginning along the Iberian rivers. On the other hand, the MPT increase in incision rates is attested all over Europe (Gibbard and Lewin, 2009). We infer that the river network has been fixed when the climate underwent larger and longer glacial/interglacial oscillations.

### 5.2 Incision: rates and significance

The incision appears to have accelerated for the last million years. In the center of the basin, around Zaragoza, the youngest endorheic sediments are currently lying at an elevation of ~700 m (Pérez-Rivarés *et al.*, 2002, 2004; Vázquez-Urbez *et al.*, 2013), ~500 m above the nearby Ebro river. A and B terraces lying 200–220 m and 140 m above Ebro river, respectively. The total amount of incision is ~300 m between the Ebro Basin opening (13–7.5 Ma) and the topmost terraces A. This is a minimum, given the possibility these strata have been buried under a couple of hundreds of meters of younger sediments before being exhumed (García-Castellanos and

**Table 4.** Synthesis of terrace level ages, from this study and literature.

| Terrace level | Median elevation above current river (m) | Published age | Method | Reference | This study | Conclusions/Adopted age |
|---|---|---|---|---|---|---|
| A | | | | | TARA0: 4731 ± 1447 ka (P-PINI) | 2800 ± 700 Ma |
| | 210 (Zaragoza area) | | | | TARA2: 2215 ± 778 ka (P-PINI) | |
| | 130 (Aragón) | | | | Mean*: 2780 ± 690 ka | |
| B | 150–180 (North-East) | 1276 ± 104 ka | ESR | Duval *et al.*, 2017 | TALC1: 5016 ± 1702 ka (P-PINI) | 1150 ± 150 ka† |
| | 140 (Ebro between Zaragoza and Aragón) | [999–1070] ka | Tentative age from paleomagnetic data | Lewis *et al.*, 2017 | TEBR2: 1034 ± 275 ka (P-PINI) | |
| | 90 (Aragón) | > 780 ka | Paleomagnetism | Lewis *et al.*, 2017 | TOJA1: 957 ± 161 ka (P-PINI) | |
| | 200 (Upper Ebro) | | | | TSEG2: [489–1104] ka (profile) | |
| | | | | | Mean*: 970 ± 130 ka | |
| C | 140 (North-East) | 817 ± 68 ka | ESR | Duval *et al.*, 2017 | | 850 ± 70 ka‡ |
| | 130 (Gállego) | [780–999] ka | Tentative age from paleomagnetic data | Lewis *et al.*, 2017 | | |
| | 115 (Ebro between Zaragoza and Aragón) | > 780 ka | Paleomagnetism | Lewis *et al.*, 2017 | | |
| | 170 (Upper Ebro) | | | | | |
| D | 100 (North-East) | < 780 ka | Paleomagnetism | Lewis *et al.*, 2017 | TSEG1: [523–971] ka (profile) | 650 ± 130 ka◊ |
| | 100 (Gállego) | ~ 780 ka | Paleomagnetism | Calle *et al.*, 2013 | | |
| | 80 (Ebro downstream Zaragoza) | | | | | |
| | 90 (Ebro between Zaragoza and Aragón) | | | | | |
| | 130 (Upper Ebro) | | | | | |
| E | 80 (North-East) | 401 ± 117 ka | Compilation of various data | Lewis *et al.*, 2017 | | 400 ± 120 |
| | 70 (Gállego) | | | | | |
| | 50 (Ebro between Zaragoza and Aragón) | | | | | |
| | 35–40 (Aragón) | | | | | |

* Inverse weighted average; when age range, we suppose a normal distribution. † With or without related karst data, average ~ 1150 ka; an uncertainty of 150 ka satisfactorily encompasses the various estimates. ‡ Average with uncertainty encompassing the various estimates. ◊ Value satisfying both paleomagnetic constraints and the age estimates for C and E.

Larrasoaña, 2015). Thus, in the Zaragoza area, the incision was ~ 40 m/Ma before 2.8 Ma then ~ 40 m/Ma for the period 2.8–1.15 Ma and ~ 120 m/Ma (x3) since then (Fig. 10). Along the Aragón valley, A and B are 130 m and 90 m above the current river, respectively: the incision rate varies from ~ 25 m/Ma for the period 2.8–1.15 Ma to ~ 80 m/Ma (x3, for uncertainties see Table S1, Supplementary Material) for the last 1.15 Ma (Fig. 10). We tested the robustness of these observations taking into account various ages and terrace elevation datasets presented in Figure S1 (Supplementary Material). It indicates that most of the Ebro basin rivers entrenched at a rate of 110 to 220 m/Ma. As proposed by Sancho *et al.* (2016), such a rate cannot have lasted for many millions of years, in agreement with a recent acceleration of incision. This analysis also confirms that incision acceleration may have occurred around 1 Ma ago, as shown by the two areas displaying old terraces: the lower Gállego and the Aragón valleys (Fig. S1, Supplementary Material). In the Duero basin, Rodríguez-Rodríguez *et al.* (2020) documented an increase in catchment-wide denudation rate by factor of two or three (x2 to x3) since 1 to 2 Ma. However, the authors relate this acceleration to expansion of the Duero drainage network driven by long-term base-level lowering and autogenic processes rather than to a climatic signal.

We note that the incision calculated in the Zaragoza area of 500 m is possibly underestimated if the latest pre-opening sediments have been buried before exhumation (García-Castellanos and Larrasoaña, 2015). Thus the pre-2.8 Ma period incision is (slightly?) lower than in the southern flank of the Pyrenean Axial Zone for the last 9 Ma deduced from low-temperature thermochronology (700–1600 m, equivalent to an exhumation rate of 130–500 m/Ma, Fillon *et al.*, 2013). This could be partly explained by the larger amount of sediments at the foot of the axial zone, where paleovalleys were filled by up to 2000 m of conglomeratic sediments now eroded (*e.g.* Vincent, 2001; Babault *et al.*, 2005a; Fillon *et al.*, 2013). It also indicates that Neogene erosion has been stronger at the foot of the Axial Zone than in the centre of the basin, which is consistent with a significant uplift of the Pyrenees relatively to the basin since 10 Ma (*e.g.* Conway-Jones *et al.*, 2019; Calvet *et al.*, 2020).

Most upper terraces developed at the outlet of Pyrenean streams when they enter into the Ebro sedimentary basin. Extensive terrace sequences developed similarly along rivers

flowing from the Iberian Chain to the south. Rivers flowing mainly within the Ebro Basin, in contrast, show less extensive terrace development, as along the Arba river. In the NW of the basin, a comparison between the Cidacos and Arga rivers is enlightening: despite of small length, the Cidacos river left large terraces, while the longer nearby Arga river shows sparse terraces with little lateral extent. Maybe, as the Arga is larger, it eroded more the ancient terraces and the Cidacos terrace remnants could be conceived more like pediments? Nevertheless, it suggests that large terrace sequences are found if (i) they form large/thick surfaces, and (ii) later river mobility was not sufficient to remove them.

Terrace distribution also indicates that older terraces developed preferentially out of the basin center and from east to west (Santisteban and Schulte, 2007). In the eastern part of the basin, the absence of the topmost level A, together with the location of the lower levels on top of the interfluves suggests that a large reshaping occurred at the Plio-Pleistocene transition. This reshaping may have produced a pediment landscape such as in the current Arba catchment (Centre-north of the basin). There, large pediments are found, in a depressed position relative to the Aragón terraces to the north-west. This is consistent with observations from other rivers of Europe for which slight incision documented during the Latest Pliocene/Early Pleistocene led to the development of wide and shallow valleys (Gibbard and Lewin, 2009). The east-west difference is also marked by a decrease of incision to the west, which could be explained by upstream incision wave migration, as recently documented in the Duero (Rodríguez-Rodríguez *et al.*, 2020). This incision wave is currently affecting the drainage divide between the Duero and Ebro catchments (Vacherat *et al.*, 2018; Struth *et al.*, 2019). Hence, the large and old terraces found upstream could correspond to the smooth landscape characterizing the area before Late Pliocene/Pleistocene incision. The geomorphic processes active at this time may have been diffuse, explaining the large scatter between the ages found (*cf.* burial dates of TARA0, TARA2). This upstream incision wave migration is potentially enhanced by an erosional isostatic rebound more pronounced in the center and eastern part of the basin than in the western part (García-Castellanos and Larrasoaña, 2015). This isostatically induced rebound is due to basin unfilling but can also be caused by moderate to important denudation of the Pyrenees and Central Iberian Massif in Plio-Pleistocene times (García-Castellanos and Larrasoaña, 2015; Stange *et al.*, 2016). In the center-east part of the basin, this uplift does not necessarily differ from the center of the basin to the Pyrenees foothills, explaining why terrace levels are parallel such as for the Segre and its tributaries (Fig. 7b). This observation seems to be valid also for the Gállego river (Fig. 7c), despite the karstic deformation occurring in its lower reaches (Benito *et al.*, 1998, 2000, Guerrero *et al.*, 2008, 2013). To the west, the Aragón river terraces show a clear decreasing incision trend downstream (Fig. 7e), while the trend is opposite along the upper Ebro River (*e.g.* the Oja/Najerilla system near the Ebro-Duero drainage divide). This trend is however not well resolved and would need additional works if we are to discuss its correlation with the post-Miocene tilt shown by lacustrine strata covering the Ebro and Duero basins (García-Castellanos and Larrasoaña, 2015). At a shorter time scale, incision rates significantly increased as already noted by Sancho *et al.* (2016). Post MPT increased erosion is likely controlled by erosion waves characterized by knickpoints migrating upstream, possibly originated at the coast as a consequence of eustatic fluctuations (*e.g.* Antoine *et al.*, 2000; Crosby and Whipple, 2006; Bridgland and Westaway, 2008; Loget and Van Den Driessche, 2009). While migrating upstream, the amplitude of erosion waves could be attenuated with higher incision rates downstream as recently documented on the Duero (Rodríguez-Rodríguez *et al.*, 2020). Hence, the more pronounced incision in the east of the basin may be driven by a position closer to the Mediterranean Sea, possibly enhanced by a Quaternary flexural erosional uplift of the entire basin up to the Catalan Coastal Range (Lewis *et al.*, 2000; Stange *et al.*, 2016).

## 6 Conclusion

A unified fluvial terrace chronology and mapping have been produced for the Ebro Basin. It is based on a review of ages from the literature and new cosmogenic nuclide ages obtained with the profile and P-PINI methods. From the topmost terrace downward, the terraces are labelled in alphabetical order. Terraces A, B, C, D, and E are dated to $2.8 \pm 0.7$ Ma, $1.15 \pm 0.15$ Ma, $850 \pm 70$ ka, $650 \pm 130$ ka and $400 \pm 120$ ka, respectively, in agreement with other dated terraces in the Iberian Peninsula and around the Pyrenees. The oldest ones (A, B, and C) are extensive, testifying for wandering fluvial systems while from D to present, the network has been stabilized and is currently entrenched in 100 to 200 m-deep valleys. We therefore hypothesize that a transition occurred from mobile to localized fluvial network. We propose this transition is likely related to the Middle Pleistocene Transition (MPT, between 0.7 and 1.3 Ma), when long-period/high-intensity climate fluctuations were established in Europe. We estimate that between 2.8–1.15 Ma and present, the incision rates have tripled, from 25–40 m/Ma to 80–120 m/Ma. After the MPT, the terrace disposition also shows more important incision and basin unfilling in the east possibly enhanced by flexural rebound.

## Supplementary Material

Supplementary Material: Tables S1–S2 and Figures S1–S17. The Supplementary Material is available at http://www.bsgf.fr/10.1051/bsgf/2021020/olm.

*Acknowledgements.* V. Zavala and J. Rat participated to the field work. We thank M. Delmas, R. Braucher, and S. Carretier for fruitful discussions. This work benefited from support and funding by OROGEN TOTAL-BRGM-CNRS project. We thank two reviewers, M. Calvet and D. García-Castellanos, and Editor A. Teixell for their careful reading and constructive comments.

## References

Alberto F, Gutiérrez M, Ibáñez MJ, Machín J, Meléndez A, Peña J, *et al.* 1983. El piedemonte pliocuaternario en el sector central pirenaico (Huesca y Lérida). *Geographicalia* 109–126.

Anderson RS, Repka JL, Dick GS. 1996. Explicit treatment of inheritance in dating depositional surfaces using in situ $^{10}$Be and $^{26}$Al. *Geology* 24: 47–51.

Antoine P, Lautridou JP, Laurent M. 2000. Long-term fluvial archives in NW France: response of the Seine and Somme rivers to tectonic movements, climatic variations and sea-level changes. *Geomorphology* 33: 183–207.

Arasa-Tuliesa A, Cabrera L. 2018. Neogene-Quaternary onshore record in the lower Ebro river incised palaeovalley (Ebro margin, Catalan Coastal Range, NE Iberia). *Geologica Acta* 16: 265–292, I–XII. https://doi.org/10.1344/GeologicaActa2018.16.3.3.

Arboleya M-L, Babault J, Owen LA, Teixell A, Finkel RC. 2008. Timing and nature of Quaternary fluvial incision in the Ouarzazate foreland basin, Morocco. *Journal of the Geological Society* 165: 1059–1073. https://doi.org/10.1144/0016-76492007-151.

Arnold M, Merchel S, Bourlès DL, Braucher R, Benedetti L, Finkel RC, *et al.* 2010. The French accelerator mass spectrometry facility ASTER: Improved performance and developments. *Nuclear Instruments and Methods in Physics Research Section B: Beam Interactions with Materials and Atoms* 268: 1954–1959. https://doi.org/10.1016/j.nimb.2010.02.107.

Babault J, Bonnet S, Crave A, Van den Driessche J. 2005a. Influence of piedmont sedimentation on erosion dynamics of an uplifting landscape: An experimental approach. *Geology* 33: 301–304.

Babault J, Van den Driessche J, Bonnet S, Castelltort S, Crave A. 2005b. Origin of the highly elevated Pyrenean peneplain. *Tectonics* 24.

Balco G, Rovey CW. 2008. An isochron method for cosmogenic-nuclide dating of buried soils and sediments. *American Journal of Science* 308: 1083–1114. https://doi.org/10.2475/10.2008.02.

Balco G, Shuster DL. 2009. $^{26}$Al–$^{10}$Be–$^{21}$Ne burial dating. *Earth and Planetary Science Letters* 286: 570–575. https://doi.org/10.1016/j.epsl.2009.07.025.

Barrón E, Rivas-Carballo R, Postigo-Mijarra JM, Alcalde-Olivares C, Vieira M, Castro L, *et al.* 2010. The Cenozoic vegetation of the Iberian Peninsula: A synthesis. *Review of Palaeobotany and Palynology* 162: 382–402. https://doi.org/10.1016/j.revpalbo.2009.11.007.

Baynes ERC, Lague D, Steer P, Bonnet S, Illien L. 2020. Sediment flux-driven channel geometry adjustment of bedrock and mixed gravel–bedrock rivers. *Earth Surface Processes and Landforms* 45: 3714–3731. https://doi.org/10.1002/esp.4996.

Beamud E, Garcés M, Cabrera L, Anton Muñoz J, Almar Y. 2003. A new middle to late Eocene continental chronostratigraphy from NE Spain. *Earth and Planetary Science Letters* 216: 501–514, https://doi.org/10.1016/S0012-821X(03)00539-9.

Beamud E, Muñoz JA, Fitzgerald PG, Baldwin SL, Garcés M, Cabrera L, *et al.* 2011. Magnetostratigraphy and detrital apatite fission track thermochronology in syntectonic conglomerates: constraints on the exhumation of the South-Central Pyrenees: South-Central Pyrenees magnetostratigraphy and thermochronology. *Basin Research* 23: 309–331. https://doi.org/10.1111/j.1365-2117.2010.00492.x.

Beaumont C, Muñoz JA, Hamilton J, Fullsack P. 2000, Factors controlling the Alpine evolution of the central Pyrenees inferred from a comparison of observations and geodynamical models. *Journal of Geophysical Research: Solid Earth* 105: 8121–8145. https://doi.org/10.1029/1999JB900390.

Benito G, Pérez-González A, Gutiérrez F, Machado MJ. 1998. River response to Quaternary subsidence due to evaporite solution (Gállego River, Ebro Basin, Spain). *Geomorphology* 22: 243–263. https://doi.org/10.1016/S0169-555X(97)00088-3.

Benito G, Gutiérrez F, Pérez-González A, Machado MJ. 2000. Geomorphological and sedimentological features in Quaternary fluvial systems affected by solution-induced subsidence (Ebro Basin, NE-Spain). *Geomorphology* 33: 209–224.

Benito G, Sancho C, Peña JL, Machado MJ, Rhodes EJ. 2010. Large-scale karst subsidence and accelerated fluvial aggradation during MIS6 in NE Spain: climatic and paleohydrological implications. *Quaternary Science Reviews* 29: 2694–2704. https://doi.org/10.1016/j.quascirev.2010.06.020.

Bessais E, Cravatte J. 1988. Les écosystèmes végétaux Pliocènes de catalogne méridionale. Variations latitudinales dans le domaine nord-ouest méditerranéen. *Geobios* 21: 49–63. https://doi.org/10.1016/S0016-6995(88)80031-7.

Bierman PR, Gillespie AR, Caffee MW. 1995. Cosmogenic Ages for Earthquake Recurrence Intervals and Debris Flow Fan Deposition, Owens Valley, California. *Science* 270: 447–450.

Bomer B. 1979. Les Piedmonts du Bassin de l'Ebre (Espagne). *Méditerranée* 36: 19–25. https://doi.org/10.3406/medit.1979.2178.

Bosch GV, Teixell A, Jolivet M, Labaume P, Stockli D, Domènech M, *et al.* 2016. Timing of Eocene-Miocene thrust activity in the Western Axial Zone and Chaînons Béarnais (west-central Pyrenees) revealed by multi-method thermochronology. *Comptes Rendus Geoscience* 348: 246–256. https://doi.org/10.1016/j.crte.2016.01.001.

Boschi L, Faccenna C, Becker TW. 2010. Mantle structure and dynamic topography in the Mediterranean Basin: mediterranean mantle and topography. *Geophysical Research Letters* 37: n/a–n/a. https://doi.org/10.1029/2010GL045001.

Braucher R, Guillou V, Bourlès DL, Arnold M, Aumaître G, Keddadouche K, *et al.* 2015. Preparation of ASTER in-house $^{10}$Be/$^{9}$Be standard solutions. *Nuclear Instruments and Methods in Physics Research Section B: Beam Interactions with Materials and Atoms* 361: 335–340. https://doi.org/10.1016/j.nimb.2015.06.012.

Bridgland, D, Westaway, R, 2008. Climatically controlled river terrace staircases: A worldwide Quaternary phenomenon. *Geomorphology* 98: 285–315. https://doi.org/10.1016/j.geomorph.2006.12.032.

Brown ET, Bourles DL, Raisbeck GM, Yiou F, Clark Burchfiel B, Molnar P, *et al.* 1998. Estimation of slip rates in the southern Tien Shan using cosmic ray exposure dates of abandoned alluvial fans. *Geological Society of America Bulletin* 110: 377–386.

Bufe A, Paola C, Burbank DW. 2016. Fluvial bevelling of topography controlled by lateral channel mobility and uplift rate. *Nature Geoscience* 9: 706–710. https://doi.org/10.1038/ngeo2773.

Bufe A, Burbank DW, Liu L, Bookhagen B, Qin J, Chen J, *et al.* 2017. Variations of Lateral Bedrock Erosion Rates Control Planation of Uplifting Folds in the Foreland of the Tian Shan, NW China. *Journal of Geophysical Research: Earth Surface* 122: 2431–2467. https://doi.org/10.1002/2016JF004099.

Calle M, Sancho C, Peña JL, Proença Cunha P, Oliva-Urcia B, Pueyo EL. 2013. La secuencia de terrazas cuaternarias del río Alcanadre (provincia de Huesca): caracterización y consideraciones medioambientales. *Cuadernos de Investigación Geográfica* 39: 159–178. https://doi.org/10.18172/cig.2004.

Calvet M, Gunnell Y, Braucher R, Hez G, Bourlès D, Guillou V, *et al.* 2015. Cave levels as proxies for measuring post-orogenic uplift: Evidence from cosmogenic dating of alluvium-filled caves in the French Pyrenees. *Geomorphology* 246: 617–633. https://doi.org/10.1016/j.geomorph.2015.07.013.

Calvet M, Gunnell Y, Laumonier B. 2020. Denudation history and palaeogeography of the Pyrenees and their peripheral basins: an 84-million-year geomorphological perspective. *Earth-Science Reviews* 103436. https://doi.org/10.1016/j.earscirev.2020.103436.

Carola E, Muñoz JA, Roca E. 2015. The transition from thick-skinned to thin-skinned tectonics in the Basque-Cantabrian Pyrenees: the Burgalesa Platform and surroundings. *International Journal of Earth Sciences* 104: 2215–2239. https://doi.org/10.1007/s00531-015-1177-z.

Casas AM, Gil I, Leránoz B, Millán H, Simón L. 1994. Quaternary reactivation of flexural-slip folds by diapiric activity: example from the

western Ebro Basin (Spain). *Geologische Rundschau* 83: 853–867. https://doi.org/10.1007/BF00251081.

Choukroune P. 1989. Étude Continentale et Océanique par Reflexion et Refraction Sismique (ECORS) Team, The ECORS Pyrenean deep seismic profiles reflection data and the overall structure of an orogenic belt. *Tectonics* 8: 23–39.

Chumakov IS. 1967, Pliocene and Pleistocene deposits of the Nile valley in Nubian and Upper Egypt (in Russian). *Geol Institute Trans, Acad Science USSR, Moscow* 170: 5.

Cloetingh S, Burov E, Beekman F, Andeweg B, Andriessen M, García-Castellanos D, *et al.* 2002. Lithospheric folding in Iberia. *Tectonics* 21(1): 5–26. https://doi.org/10.1029/2001TC901031.

Coney PJ, Muñoz JA, McClay KR, Evenchick CA. 1996. Syntectonic burial and post-tectonic exhumation of the southern Pyrenees foreland fold-thrust belt. *Journal of the Geological Society* 153: 9–16. https://doi.org/10.1144/gsjgs.153.1.0009.

Conway-Jones BW, Roberts GG, Fichtner A, Hoggard M. 2019. Neogene Epeirogeny of Iberia. *Geochemistry, Geophysics, Geosystems* 20: 1138–1163. https://doi.org/10.1029/2018GC007899.

Cook KL, Turowski JM, Hovius N. 2014. River gorge eradication by downstream sweep erosion. *Nature Geoscience* 7: 682–686. https://doi.org/10.1038/ngeo2224.

Cordier S, Adamson K, Delmas M, Calvet M, Harmand D. 2017. Of ice and water: Quaternary fluvial response to glacial forcing. *Quaternary Science Reviews* 166: 57–73. https://doi.org/10.1016/j.quascirev.2017.02.006.

Costa E, Garcés M, López-Blanco M, Beamud E, Gómez-Paccard M, Larrasoaña JC. 2010. Closing and continentalization of the South Pyrenean foreland basin (NE Spain): magnetochronological constraints. *Basin Research* 22: 904–917. https://doi.org/10.1111/j.1365-2117.2009.00452.x.

Craddock WH, Kirby E, Harkins NW, Zhang H, Shi X, Liu J. 2010. Rapid fluvial incision along the Yellow River during headward basin integration. *Nature Geoscience* 3: 209–213. https://doi.org/10.1038/ngeo777.

Crosby BT, Whipple KX. 2006. Knickpoint initiation and distribution within fluvial networks: 236 waterfalls in the Waipaoa River, North Island, New Zealand. *Geomorphology* 82: 16–38. https://doi.org/10.1016/j.geomorph.2005.08.023.

Crosby BT, Whipple KX, Gasparini NM, Wobus CW. 2007. Formation of fluvial hanging valleys: Theory and simulation. *Journal of Geophysical Research* 112: F03S10. https://doi.org/10.1029/2006JF000566.

Del Rio P, Barbero L, Stuart F. 2009. Exhumation of the Sierra de Cameros (Iberian Range, Spain): constraints from low-temperature thermochronology. *Geological Society, London, Special Publications* 324: 153–166.

Delmas M. 2019. L'apport des nucléides cosmogéniques produits in situ à la quantification multi-scalaire des changements environnementaux quaternaires dans les montagnes des latitudes tempérées [HDR]. Université Lumière Lyon 2.

Delmas M, Calvet M, Gunnell Y, Voinchet P, Manel C, Braucher R, *et al.* 2018. Terrestrial 10Be and electron spin resonance dating of fluvial terraces quantifies quaternary tectonic uplift gradients in the eastern Pyrenees. *Quaternary Science Reviews* 193: 188–211. https://doi.org/10.1016/j.quascirev.2018.06.001.

Dunai TJ. 2010. Cosmogenic nuclides: principles, concepts and applications in the earth surface sciences. Cambridge, New York: Cambridge University Press. http://dx.doi.org/10.1017/CBO9780511804519 (accessed August 2017).

Duval M, Sancho C, Calle M, Guilarte V, Peña-Monné JL. 2015. On the interest of using the multiple center approach in ESR dating of optically bleached quartz grains: Some examples from the Early Pleistocene terraces of the Alcanadre River (Ebro basin, Spain). *Quaternary Geochronology* 29: 58–69. https://doi.org/10.1016/j.quageo.2015.06.006.

Duval M, Arnold LJ, Guilarte V, Demuro M, Santonja M, Pérez-González A. 2017. Electron spin resonance dating of optically bleached quartz grains from the Middle Palaeolithic site of Cuesta de la Bajada (Spain) using the multiple centres approach. *Quaternary Geochronology* 37: 82–96. https://doi.org/10.1016/j.quageo.2016.09.006.

Etheve N, Mohn G, Lamotte DF de, Roca E, Tugend J, Gómez-Romeu J. 2018. Extreme Mesozoic Crustal Thinning in the Eastern Iberia Margin: The Example of the Columbrets Basin (Valencia Trough). *Tectonics* 37: 636–662. https://doi.org/10.1002/2017TC004613.

Evans G, Arche A. 2002. The flux of siliciclastic sediment from the Iberian Peninsula, with particular reference to the Ebro. *Geological Society, London, Special Publications* 191: 199–208.

Faccenna C, *et al.* 2014. Mantle dynamics in the Mediterranean: mediterranean dynamic. *Reviews of Geophysics* 52: 283–332. https://doi.org/10.1002/2013RG000444.

Fillon C, Gautheron C, van der Beek P. 2013. Oligocene–Miocene burial and exhumation of the Southern Pyrenean foreland quantified by low-temperature thermochronology. *Journal of the Geological Society* 170: 67–77.

Fillon C, Pedreira D, van der Beek PA, Huismans RS, Barbero L, Pulgar JA. 2016. Alpine exhumation of the central Cantabrian Mountains, Northwest Spain: alpine exhumation of the cantabrians. *Tectonics* 35: 339–356. https://doi.org/10.1002/2015TC004050.

Fillon C, *et al.* 2020. Post-orogenic exhumation in the western Pyrenees: evidence for extension driven by pre-orogenic inheritance. *Journal of the Geological Society*. https://doi.org/10.1144/jgs2020-079.

Fitzgerald PG, Muñoz JA, Coney PJ, Baldwin SL. 1999. Asymmetric exhumation across the Pyrenean orogen: implications for the tectonic evolution of a collisional orogen. *Earth and Planetary Science Letters* 173: 157–170. https://doi.org/10.1016/S0012-821X(99)00225-3.

Fontboté J, Guimerà J, Roca E, Sàbat F, Santanach P, Fernández-Ortigosa F. 1990. The Cenozoic geodynamic evolution of the Valencia trough (western Mediterranean). *Rev. Soc. Geol. Esp.* 3: 249–259.

Fornari M, Risacher F, Féraud G. 2001. Dating of paleolakes in the central Altiplano of Bolivia. *Palaeogeography, Palaeoclimatology, Palaeoecology* 172: 269–282. https://doi.org/10.1016/S0031-0182(01)00301-7.

Fuller IC, Macklin MG, Passmore DG, Brewer PA, Lewin J, Wintle AG. 1996. Geochronologies and environmental records of Quaternary fluvial sequences in the Guadalope basin, northeast Spain, based on luminescence dating. *Geological Society, London, Special Publications* 115: 99–120. https://doi.org/10.1144/GSL.SP1996.115.01.09.

Fuller IC, Macklin MG, Lewin J, Passmore DG, Wintle AG. 1998. River response to high-frequency climate oscillations in southern Europe over the past 200 k.y. *Geology* 26: 275–278. https://doi.org/10.1130/0091-7613(1998)026<0275:RRTHFC>2.3.CO;2.

García-Castellanos D. 2006. Long-term evolution of tectonic lakes: climatic controls on the development of internally drained basins. *Special Papers-Geological Society of America* 398: 283.

García-Castellanos D, Larrasoaña JC. 2015. Quantifying the post-tectonic topographic evolution of closed basins: The Ebro basin (northeast Iberia). *Geology* 43: 663–666. https://doi.org/10.1130/G36673.1.

García-Castellanos D, Vergés J, Gaspar-Escribano J, Cloetingh S. 2003. Interplay between tectonics, climate, fluvial transport during

the Cenozoic evolution of the Ebro Basin (NE Iberia). *Tectonics, Climate, Drainage: Journal of Geophysical Research: Solid Earth* 108. https://doi.org/10.1029/2002JB002073.

García-Ruiz JM, Martí-Bono C, Peña-Monné JL, Sancho C, Rhodes EJ, Valero-garcés B, *et al.* 2013. Glacial and fluvial deposits in the aragón valley, central-western Pyrenees: chronology of the pyrenean late pleistocene glaciers. *Geografiska Annaler: Series A, Physical Geography* 95: 15–32. https://doi.org/10.1111/j.1468-0459.2012.00478.x.

Gaspar-Escribano JM, García-Castellanos D, Roca E, Cloetingh S. 2004. Cenozoic vertical motions of the Catalan Coastal Ranges (NE Spain): The role of tectonics, isostasy, surface transport. *Tectonics* 23. https://doi.org/10.1029/2003TC001511.

Genti M. 2015. Impact des processus de surface sur la déformation actuelle des Pyrénées et des Alpes. PhD Thesis, Université de Montpellier, 263 p.

Gibbard PL, Lewin J. 2009. River incision and terrace formation in the Late Cenozoic of Europe. *Tectonophysics* 474: 41–55. https://doi.org/10.1016/j.tecto.2008.11.017.

Gibson M, Sinclair HD, Lynn GJ, Stuart FM. 2007. Late- to post-orogenic exhumation of the Central Pyrenees revealed through combined thermochronological data and modelling. *Basin Research* 19: 323–334. https://doi.org/10.1111/j.1365-2117.2007.00333.x.

Gosse JC, Phillips FM. 2001. Terrestrial in situ cosmogenic nuclides: theory and application. *Quaternary Science Reviews* 20: 1475–1560.

Guerrero J, Gutiérrez F, Lucha P. 2008. Impact of halite dissolution subsidence on Quaternary fluvial terrace development: Case study of the Huerva River, Ebro Basin, NE Spain. *Geomorphology* 100: 164–179. https://doi.org/10.1016/j.geomorph.2007.04.040.

Guerrero J, Gutiérrez F, Galve JP. 2013. Large depressions, thickened terraces, gravitational deformation in the Ebro River valley (Zaragoza area, NE Spain): Evidence of glauberite and halite interstratal karstification. *Geomorphology* 196: 162–176. https://doi.org/10.1016/j.geomorph.2012.06.024.

Han Z, *et al.* 2019. Internal Drainage Has Sustained Low-Relief Tibetan Landscapes Since the Early Miocene. *Geophysical Research Letters* 46: 8741–8752. https://doi.org/10.1029/2019GL083019.

Haug GH, Tiedemann R. 1998. Effect of the formation of the Isthmus of Panama on Atlantic Ocean thermohaline circulation. *Nature* 393: 673–676.

Hidy AJ, Gosse JC, Pederson JL, Mattern JP, Finkel RC. 2010. A geologically constrained Monte Carlo approach to modeling exposure ages from profiles of cosmogenic nuclides: An example from Lees Ferry, Arizona. *Geochemistry Geophysics Geosystems* 11. https://doi.org/10.1029/2010GC003084.

Huyghe D, Mouthereau F, Ségalen L, Furió M. 2020. Long-term dynamic topographic support during post-orogenic crustal thinning revealed by stable isotope (δ18O) paleo-altimetry in eastern Pyrenees. *Scientific Reports* 10. https://doi.org/10.1038/s41598-020-58903-w.

Jiménez-Moreno G, Burjachs F, Expósito I, Oms O, Carrancho Á, Villalaín JJ, *et al.* 2013. Late Pliocene vegetation and orbital-scale climate changes from the western Mediterranean area. *Global and Planetary Change* 108: 15–28.

Jolivet M, Labaume P, Monié P, Brunel M, Arnaud N, Campani M. 2007. Thermochronology constraints for the propagation sequence of the south Pyrenean basement thrust system (France-Spain). *Tectonics* 26.

Julián Andrés A. 1996. Cartografía y correlación general de las acumulaciones cuaternarias de la depresión del Ebro. PhD Thesis, Universidad de Zaragoza.

Julián Andrés A, Chueca Cía JJ. 1998. Acumulaciones fluviales en la Depresión del Ebro: valoración de la validez de una secuencia general. *Geographicalia* 67–82.

Jungers MC, Heimsath AM. 2016. Post-tectonic landscape evolution of a coupled basin and range: Pinaleño Mountains and Safford Basin, southeastern Arizona. *Geological Society of America Bulletin* 128: 469–86. https://doi.org/10.1130/B31276.1.

Knudsen MF, Nørgaard J, Grischott R, Kober F, Egholm DL, Hansen TM, *et al.* 2020. New cosmogenic nuclide burial-dating model indicates onset of major glaciations in the Alps during Middle Pleistocene Transition. *Earth and Planetary Science Letters* 549: 116491. https://doi.org/10.1016/j.epsl.2020.116491.

Labaume P, Meresse F, Jolivet M, Teixell A, Lahfid A. 2016. Tectonothermal history of an exhumed thrust-sheet-top basin: An example from the south Pyrenean thrust belt. *Tectonics* 35: 1280–1313. https://doi.org/10.1002/2016TC004192.

Lal D. 1991. Cosmic ray labeling of erosion surfaces: in-situ nuclide production rates and erosion models. *Earth Planet. Sci. Lett.* 104: 424–439.

Larrasoaña JC, Murelaga X, Garcés M. 2006. Magnetobiochronology of Lower Miocene (Ramblian) continental sediments from the Tudela Formation (western Ebro basin, Spain). *Earth and Planetary Science Letters* 243: 409–423. https://doi.org/10.1016/j.epsl.2006.01.034.

Lewis CJ, Vergés J, Marzo M. 2000. High mountains in a zone of extended crust: Insights into the Neogene-Quaternary topographic development of northeastern Iberia. *Tectonics* 19: 86–102. https://doi.org/10.1029/1999TC900056.

Lewis CJ, McDonald EV, Sancho C, Peña JL, Rhodes EJ. 2009. Climatic implications of correlated Upper Pleistocene glacial and fluvial deposits on the Cinca and Gállego Rivers (NE Spain) based on OSL dating and soil stratigraphy. *Global and Planetary Change* 67: 141–152. https://doi.org/10.1016/j.gloplacha.2009.01.001.

Lewis CJ, Sancho C, McDonald EV, Peña-Monné JL, Pueyo EL, Rhodes E, *et al.* 2017. Post-tectonic landscape evolution in NE Iberia using staircase terraces: Combined effects of uplift and climate. *Geomorphology* 292: 85–103. https://doi.org/10.1016/j.geomorph.2017.04.037.

Lisiecki LE, Raymo ME. 2005. A Pliocene-Pleistocene stack of 57 globally distributed benthic delta O-18 records (vol 20, art no PA1003, 2005). *Paleoceanography* 20: PA2007. https://doi.org/10.1029/2005PA001164.

Loget N, Van Den Driessche J. 2009. Wave train model for knickpoint migration. *Geomorphology* 106: 376–382.

Loget N, Driessche JVD, Davy P. 2005. How did the Messinian salinity crisis end? *Terra Nova* 17: 414–419.

López Martínez N, Agustí J, Cabrera L, Calvo Sorando J, Civis J, Corrochano A, *et al.* 1987. Approach to the Spanish continental Neogene synthesis and palaeoclimatic interpretation. *Ann. Inst. Geol. Publ. Hung* LXX: 383–391.

López-Blanco M. 2002. Sedimentary response to thrusting and fold growing on the SE margin of the Ebro basin (Paleogene, NE Spain). *Sedimentary Geology* 146: 133–154.

Lucha P, Gutiérrez F, Galve JP, Guerrero J. 2012. Geomorphic and stratigraphic evidence of incision-induced halokinetic uplift and dissolution subsidence in transverse drainages crossing the evaporite-cored Barbastro-Balaguer Anticline (Ebro Basin, NE Spain). *Geomorphology* 171-172: 154–172. https://doi.org/10.1016/j.geomorph.2012.05.015.

Macklin MG, Fuller IC, Lewin J, Maas GS, Passmore DG, Rose J, *et al.* 2002. Correlation of fluvial sequences in the Mediterranean basin over the last 200 ka and their relationship to climate change. *Quaternary Sci. Rev.* 21: 1633–1641.

Maier-Reimer E, Mikolajewicz U, Crowley T. 1990. Ocean general circulation model sensitivity experiment with an open Central American Isthmus. *Paleoceanography* 5: 349–366.

Mensua S, Ibañez MJ. 1977. Terrazas y glacis del centro de la depresion del Ebro (5 mapas y Comentario). Departamento de Geografia.

Mocochain L, Audra P, Clauzon G, Bellier O, Bigot J-Y, Parize O, *et al.* 2009. The effect of river dynamics induced by the Messinian Salinity Crisis on karst landscape and caves: example of the Lower Ardèche river (mid Rhône valley). *Geomorphology* 106: 46–61.

Molnar P. 2008. Closing of the Central American Seaway and the Ice Age: A critical review. *Paleoceanography* 23.

Monod B, Regard V, Carcone J, Wyns R, Christophoul F. 2016. Postorogenic planar palaeosurfaces of the central Pyrenees: Weathering and neotectonic records. *Comptes Rendus Geoscience* 348: 184–193. https://doi.org/10.1016/j.crte.2015.09.005.

Moreno D, *et al.* 2012. ESR chronology of alluvial deposits in the Arlanzón valley (Atapuerca, Spain): Contemporaneity with Atapuerca Gran Dolina site. *Quaternary Geochronology* 10: 418–423. https://doi.org/10.1016/j.quageo.2012.04.018.

Morris, Sinclair, Yell. 1998. Exhumation of the Pyrenean orogen: implications for sediment discharge. *Basin Research* 10: 69–85. https://doi.org/10.1046/j.1365-2117.1998.00053.x.

Mouthereau F, Filleaudeau P-Y, Vacherat A, Pik R, Lacombe O, Fellin MG, *et al.* 2014. Placing limits to shortening evolution in the Pyrenees: Role of margin architecture and implications for the Iberia/Europe convergence: Plate convergence in the Pyrenees. *Tectonics* 33: 2283–2314. https://doi.org/10.1002/2014TC003663.

Muñoz JA. 1992. Evolution of a continental collision belt: ECORS-Pyrenees crustal balanced cross-section. In: Thrust tectonics. Springer, pp. 235–246.

Muñoz J, Martínez A, Vergés J. 1986. Thrust sequences in the eastern Spanish Pyrenees. *Journal of Structural Geology* 8: 399–405.

Peña-Monné J, Sancho C. 1988. Correlación y evolución cuaternaria del sistema fluvial Segre-Cinca en su curso bajo (provs. de Lérida y Huesca). *Cuaternario y geomorfología* 2: 77–83.

Pérez-Rivarés F, Garcés M, Arenas C, Pardo G. 2002. Magneto-cronología de la sucesión miocena de la Sierra de Alcubierre (sector central de la Cuenca del Ebro). *Revista de la Sociedad Geológica de España* 15: 217–231.

Pérez-Rivarés J, Crespo MG, Abad MCA, Tirapu GP. 2004. Magnetostratigraphy of the Miocene continental deposits of the Montes de Castejón (central Ebro basin, Spain): geochronological and paleoenvironmental implications. *Geologica Acta* 2: 221–234.

Puigdefàbregas C, Muñoz JA, Vergés J. 1992. Thrusting and foreland basin evolution in the Southern Pyrenees. In: McClay KR, ed. Thrust Tectonics. Dordrecht: Springer Netherlands, pp. 247–254. https://doi.org/10.1007/978-94-011-3066-0_22.

Rat J, Mouthereau F, Brichau S, Crémades A, Bernet M, Balvay M, *et al.* 2019. Tectonothermal Evolution of the Cameros Basin: Implications for Tectonics of North Iberia. *Tectonics* 38: 440–469. https://doi.org/10.1029/2018TC005294.

Regard, *et al.* 2005. Cumulative right-lateral fault slip rate across the Zagros-Makran transfer zone: role of the Minab-Zendan fault system in accommodating Arabia-Eurasia convergence in south-east Iran. *Geophysical Journal International* 162: 177–203.

Repka JL, Anderson RS, Finkel RC. 1997. Cosmogenic dating of fluvial terraces, Fremont River, Utah. *Earth and Planetary Science Letters* 152: 59–73.

Ritz JF, *et al.* 2003. Late Pleistocene to Holocene slip rates for the Gurvan Bulag thrust fault (Gobi-Altay, Mongolia) estimated with Be-10 dates. *Journal of Geophysical Research-Solid Earth* 108.

Roca E, Guimerà J. 1992. The Neogene structure of the eastern Iberian margin: Structural constraints on the crustal evolution of the Valencia trough (western Mediterranean). *Tectonophysics* 203: 203–218. https://doi.org/10.1016/0040-1951(92)90224-T.

Roca E, Desegaulx P, Fernandez Ortigosa F, Roure F, Pinet B. 1990. In: Pinet B, Bois C, eds. The Potential of Deep Seismic Profiling for Hydrocarbon Exploration. *Proceedings of the 5th IFP Exploration and Production Research Conference, held in Arles, June 19–23, 1989*, Paris, pp. 439–443.

Roca E, Sans M, Cabrera L, Marzo M. 1999. Oligocene to Middle Miocene evolution of the central Catalan margin (northwestern Mediterranean). *Tectonophysics* 315: 209–229. https://doi.org/10.1016/S0040-1951(99)00289-9.

Rodríguez-Rodríguez L, *et al.* 2020. Dates and rates of endo-exorheic drainage development: Insights from fluvial terraces (Duero River, Iberian Peninsula). *Global and Planetary Change* 193: 103271. https://doi.org/10.1016/j.gloplacha.2020.103271.

Roure F, Choukroune P, Berastegui X, Munoz J, Villien A, Matheron P, *et al.* 1989. ECORS deep seismic data and balanced cross sections: Geometric constraints on the evolution of the Pyrenees. *Tectonics* 8: 41–50.

Rushlow CR, Barnes JB, Ehlers TA, Vergés J. 2013. Exhumation of the southern Pyrenean fold-thrust belt (Spain) from orogenic growth to decay. *Tectonics* 32: 843–860. https://doi.org/10.1002/tect.20030.

Sàbat F, Roca E, Muñoz J, Vergés J, Santanach P, Sans M. 1995. margin of Iberia: the ESCI-València Trough seismic profile. *Rev. Soc. Geol. Esp.* 8: 4.

Salas R, Casas A. 1993. Mesozoic extensional tectonics, stratigraphy and crustal evolution during the Alpine cycle of the eastern Iberian basin. *Tectonophysics* 228: 33–55. https://doi.org/10.1016/0040-1951(93)90213-4.

Salas R, Guimerà J, Mas R, Martín-Closas C, Meléndez A, Alonso A. 2001. Evolution of the Mesozoic central Iberian Rift System and its Cainozoic inversion (Iberian chain). *Peri-Tethys Memoir* 6: 145–185.

Sancho C, Calle M, Pena-Monne JL, Duval M, Oliva-Urcia B, Pueyo EL, *et al.* 2016. Dating the Earliest Pleistocene alluvial terrace of the Alcanadre River (Ebro Basin, NE Spain): Insights into the landscape evolution and involved processes. *Quaternary International* 407: 86–95. https://doi.org/10.1016/j.quaint.2015.10.050.

Sancho C, Arenas C, Pardo G, Peña-Monné JL, Rhodes EJ, Bartolomé M, *et al.* 2018. Glaciolacustrine deposits formed in an ice-dammed tributary valley in the south-central Pyrenees: New evidence for late Pleistocene climate. *Sedimentary Geology* 366: 47–66. https://doi.org/10.1016/j.sedgeo.2018.01.008.

Santisteban JI, Schulte L. 2007. Fluvial networks of the Iberian Peninsula: a chronological framework. *Quaternary Science Reviews* 26: 2738–2757. https://doi.org/10.1016/j.quascirev.2006.12.019.

Saura E, Ardèvol i Oró Ll, Teixell A, Vergés J. 2016. Rising and falling diapirs, shifting depocenters, flap overturning in the Cretaceous Sopeira and Sant Gervàs subbasins (Ribagorça Basin, southern Pyrenees). *Tectonics* 35: 638–662. https://doi.org/10.1002/2015TC004001.

Siddall M, Honisch B, Waelbroeck C, Huybers P. 2010. Changes in deep Pacific temperature during the mid-Pleistocene transition and quaternary. *Quaternary Science Reviews* 29: 170–181.

Sinclair HD, Gibson M, Naylor M, Morris RG. 2005. Asymmetric growth of the Pyrenees revealed through measurement and modeling of orogenic fluxes. *American Journal of Science* 305: 369–406, https://doi.org/10.2475/ajs.305.5.369.

Sobel ER, Hilley GE, Strecker MR. 2003. Formation of internally drained contractional basins by aridity-limited bedrock incision. *Journal of Geophysical Research: Solid Earth* 108. https://doi.org/10.1029/2002JB001883.

Soria Jáuregui Á, González Amuchastegui MJ, Serrano Cañadas E, Edeso Fito JM, Lopetegi Galarraga A, Duval M, *et al.* 2019. Las terrazas fluviales cuaternarias del río Ebro en el alto Ebro (Incinillas-Conchas de Haro). Asociación Española para el Estudio del Cuaternario (AEQUA), https://cir.cenieh.es/handle/20.500.12136/1418 (accessed February 2020).

Stange KM, van Balen R, Carcaillet J, Vandenberghe J. 2013a. Terrace staircase development in the Southern Pyrenees Foreland: Inferences from $^{10}$Be terrace exposure ages at the Segre River. *Global and Planetary Change* 101: 97–112. https://doi.org/10.1016/j.gloplacha.2012.12.007.

Stange KM, van Balen R, Vandenberghe J, Peña JL, Sancho C. 2013b. External controls on Quaternary fluvial incision and terrace formation at the Segre River, Southern Pyrenees. *Tectonophysics* 602: 316–331. https://doi.org/10.1016/j.tecto.2012.10.033.

Stange KM, Balen RTV, García-Castellanos D, Cloetingh S. 2016. Numerical modelling of Quaternary terrace staircase formation in the Ebro foreland basin, southern Pyrenees, NE Iberia. *Basin Research* 28: 124–146. https://doi.org/10.1111/bre.12103.

Struth L, García-Castellanos D, Viaplana-Muzas M, Vergés J. 2019. Drainage network dynamics and knickpoint evolution in the Ebro and Duero basins: From endorheism to exorheism. *Geomorphology* 327: 554–571. https://doi.org/10.1016/j.geomorph.2018.11.033.

Suc J-P, Popescu S-M. 2005. Pollen records and climatic cycles in the North Mediterranean region since 2.7 Ma. *Geological Society, London, Special Publications* 247: 147–158.

Teixell A. 1990. Alpine thrusts at the western termination of the Pyrenean axial zone. *Bulletin de la Société Géologique de France* VI: 241–249. https://doi.org/10.2113/gssgfbull.VI.2.241.

Teixell A. 1996. The Ansó transect of the southern Pyrenees: basement and cover thrust geometries. *Journal of the Geological Society* 153: 301–310. https://doi.org/10.1144/gsjgs.153.2.0301.

Teixell A. 1998. Crustal structure and orogenic material budget in the west central Pyrenees. *Tectonics* 17: 395–406. https://doi.org/10.1029/98TC00561.

Tziperman E, Gildor H. 2003. On the mid-Pleistocene transition to 100-kyr glacial cycles and the asymmetry between glaciation and deglaciation times. *Paleoceanography* 18: 1.

Urgeles R, Camerlenghi A, García-Castellanos D, De Mol B, Garcés M, Vergés J, *et al.* 2011. New constraints on the Messinian sealevel drawdown from 3D seismic data of the Ebro Margin, western Mediterranean. *Basin Research* 23: 123–145.

Vacherat A, Bonnet S, Mouthereau F. 2018. Drainage reorganization and divide migration induced by the excavation of the Ebro basin (NE Spain). *Earth Surface Dynamics* 6: 369–387. https://doi.org/10.5194/esurf-6-369-2018.

Vázquez-Urbez M, Arenas C, Pardo G, Pérez-Rivarés J. 2013. The Effect of Drainage Reorganization and Climate On the Sedimentologic Evolution of Intermontane Lake Systems: The Final Fill Stage of the Tertiary Ebro Basin (Spain). *Journal of Sedimentary Research* 83: 562–590. https://doi.org/10.2110/jsr2013.47.

Vergés J, Millán H, Roca E, Muñoz J, Marzo M, Cirés J, *et al.* 1995. Eastern Pyrenees and related foreland basins: pre-, syn-and post-collisional crustal-scale cross-sections. *Marine and Petroleum Geology* 12: 903–915.

Vergés J, Fernàndez M, Martìnez A. 2002. The Pyrenean orogen: pre-, syn-, post-collisional evolution. *Journal of the Virtual Explorer* 8: 55–74.

Vincent SJ. 2001. The Sis palaeovalley: a record of proximal fluvial sedimentation and drainage basin development in response to Pyrenean mountain building. *Sedimentology* 48: 1235–1276, https://doi.org/10.1046/j.1365-3091.2001.00421.x.

Whitchurch AL, Carter A, Sinclair HD, Duller RA, Whittaker AC, Allen PA. 2011, Sediment routing system evolution within a diachronously uplifting orogen: Insights from detrital zircon thermochronological analyses from the South-Central Pyrenees. *American Journal of Science* 311: 442–482. https://doi.org/10.2475/05.2011.03.

Yelland A. 1990. Fission track thermotectonics in the Pyrenean orogen. *International Journal of Radiation Applications and Instrumentation. Part D. Nuclear Tracks and Radiation Measurements* 17: 293–299.

**Cite this article as**: Regard V, Vacherat A, Bonnet S, Mouthereau F, Nørgaard J, Knudsen MF. 2021. Late Pliocene-Pleistocene incision in the Ebro Basin (North Spain), *BSGF - Earth Sciences Bulletin* 192: 30.